NASA Technical Memorandum 101712

Effects of Wing Sweep on Boundary-Layer Transition for a Smooth F-14A Wing at Mach Numbers From 0.700 To 0.825

Bianca Trujillo Anderson and Robert R. Meyer, Jr.

May 1990

FEDD

FOR EARLY DOMESTIC DISSEMINATION

Because of its significant early commercial potential, this information, which has been developed under a U.S. Government program, is being disseminated within the United States in advance of general publication. This information may be duplicated and used by the recipient with the express limitation that it not be published. Release of this information to other domestic parties by the recipient shall be made subject to these limitations. Foreign release may be made only with prior NASA approval and appropriate export licenses. This legend shall be marked on any reproduction of this information in whole or in part. Date for general release May 31, 1991

NASA

National Aeronautics and
Space Administration

NASA Technical Memorandum 101712

Effects of Wing Sweep on Boundary-Layer Transition for a Smooth F-14A Wing at Mach Numbers From 0.700 To 0.825

Bianca Trujillo Anderson and Robert R. Meyer, Jr.
Ames Research Center, Dryden Flight Research Facility, Edwards, California

1990

National Aeronautics and
Space Administration
Ames Research Center
Dryden Flight Research Facility
Edwards, California 93523-0273

CONTENTS

SUMMARY 1

INTRODUCTION 1

NOMENCLATURE 2
Subscripts 3

DESCRIPTION OF THE TEST AIRCRAFT CONFIGURATION 3
F-14A Aircraft 3
Glove 1 4

INSTRUMENTATION 4
Flush Static Pressure Orifices 5
Hot-Film Anemometer Systems 5
Boundary-Layer Rakes 5
Dynamic Pressure Transducers (Microphones) 5
Charge Patch 6
Uplink Guidance System 6
Aircraft Instrumentation 6
Accuracy 6

FLIGHT-TEST CONDITIONS AND PROCEDURES 6

RESULTS AND DISCUSSION 7
Pressure Distributions 7
Transition Data 8
Trends in the Transition Database 8
Maximum Transition Locations 9
Maximum Transition Reynolds Number 9
Momentum Thickness Related to Skin Friction 10
Effects of Engine Noise on Transition 10
Effects of Cirrus Clouds on Transition 10

CONCLUDING REMARKS 11

REFERENCES 13

TABLES 14

MICROFICHE SUPPLEMENT
Table 5. Glove section pressure coefficients m-1
Table 6. Boundary-layer velocity profile data. m-1115
Table 7. Boundary-layer transition locations. m-2261

LIST OF FIGURES

Figure 1. F-14A aircraft with glove 1 on left wing. 19

Figure 2. Typical glove 1 cross section. 19

(a) Waviness measurements. 20

(b) Mechanical deflection dial gauge used to measure glove surface curvature. 20

Figure 3. Glove 1 waviness. 20

Figure 4. Glove 1 upper surface planform and instrumentation layout. 21

Figure 5. Glove 1 hot-film sensor. 21

Figure 6. Boundary-layer rake. 22

Figure 7. Charge-patch location. 23

Figure 8. Glove 1 operating envelope. 23

Figure 9. Glove 1 middle station pressure distributions; α = trim, Λ = 20°. 24

(a) Transition data. 24

Figure 10. Transition data and pressure distributions for $M = 0.700$, $\Lambda = 20°$, and hp = 35,000 ft. 24

(b) Pressure distributions, $\alpha = 0.84°$. 25

(c) Pressure distributions, $\alpha = 3.4°$. 25

(a) Transition data. 26

(b) Pressure distributions, $\alpha = 0.22°$. 26

(c) Pressure distributions, $\alpha = 1.57°$. 26

Figure 11. Transition data and pressure distributions for $M = 0.700$, $\Lambda = 35°$, and hp = 35,000 ft. . 26

(a) Transition data. 27

(b) Pressure distributions, $\alpha = 0.46°$. 27

(c) Pressure distributions, $\alpha = 1.46°$. 27

Figure 12. Transition data and pressure distributions for $M = 0.800$, $\Lambda = 20°$, and hp = 35,000 ft. 27

Figure 13. Maximum transition location as a function of sweep; M = 0.700, hp = 10,000 ft. 28

Figure 14. Maximum transition location as a function of sweep; M = 0.700, 0.750, 0.800 and hp = 20,000 ft. 29

Figure 15. Maximum transition location as a function of sweep; M = 0.700, 0.750, 0.800 and hp = 25,000 ft. 30

Figure 16. Maximum transition location as a function of sweep; M = 0.750, 0.800 and hp = 30,000 ft. 31

Figure 17. Maximum transition location as a function of sweep; M = 0.700, 0.750, 0.800 and hp = 35,000 ft. 32

Figure 18. Maximum transition Reynolds number as a function of sweep. 33

Figure 19. Momentum thickness as a function of transition location for M = 0.700, Λ = 20°, and hp = 20,000 and 35,000 ft. 34

Figure 20. Momentum thickness as a function of $(x/c)_T$, $M = 0.800$, and $\Lambda = 20°$. 34
Figure 21. Momentum thickness as a function of $(x/c)_T$, $M = 0.700$, and $\Lambda = 35°$. 35
(a) $hp = 20{,}000$ ft. 36
(b) $hp = 35{,}000$ ft. 36
Figure 22. Microphone data for $M = 0.700$ and $\Lambda = 20°$. 36
(a) $hp = 20{,}000$ ft. 37
(b) $hp = 35{,}000$ ft. 37
Figure 23. Microphone data for $M = 0.800$ and $\Lambda = 20°$. 37
(a) Normal throttle setting. 38
(b) Left engine throttled back. 38
Figure 24. Microphone data for leading-edge noise study; $M = 0.750$, $\Lambda = 30°$, and $hp = 35{,}000$ ft. 38
Figure 25. Typical cirrus clouds. 39
(a) Typical hot-film signals. 40
(b) Charge-patch signal. 40
Figure 26. Hot-film and charge-patch signals without cloud encounters. 40
(a) Hot-film signals. 41
(b) Charge-patch signal. 41
Figure 27. Hot-film and charge-patch signals with cloud encounters. 41
(a) Hot-film signals. 42
(b) Charge-patch signal. 42
Figure 28. Hot-film and charge-patch signals with cloud encounters. 42

SUMMARY

This report discusses the results of the variable-sweep transition flight experiment (VSTFE). The VSTFE was a natural laminar flow experiment flown on the swing-wing F-14A aircraft. The main objective of the VSTFE was to determine the effects of wing sweep on boundary-layer transition at conditions representative of transport aircraft. The experiment included the flight-testing of two laminar-flow wing gloves. Glove 1 was a cleanup of the existing F-14A wing. Glove 2, not discussed in this report, was designed to provide favorable pressure distributions for natural laminar flow at Mach number (M) 0.700.

The transition locations presented for glove 1 were determined primarily by using hot-film sensors. Boundary-layer rake data was provided as a supplement. Transition data were obtained for leading-edge wing sweeps of 15°, 20°, 25°, 30°, and 35°, with Mach numbers ranging from 0.700 to 0.825, and altitudes ranging from 10,000 to 35,000 ft. Results show that a substantial amount of laminar flow was maintained at all the wing sweeps evaluated. The maximum transition Reynolds number of 13.7×10^6 was obtained for the condition of 15° of sweep, M = 0.800, and an altitude of 20,000 ft.

INTRODUCTION

Retaining a laminar boundary layer over a large portion of an aircraft wing and empennage can result in appreciable drag reduction. Several studies have shown that transports of all sizes could benefit from maintaining a laminar boundary layer because of the flight time spent at steady-state cruise conditions (refs. 1–7).

Laminar flow can be achieved through active or passive means. The active method uses suction through the wing surface to maintain laminar flow to potentially 100 percent of the wing chord at very high Reynolds numbers. The passive method requires proper shaping of the wing to obtain a pressure distribution with a favorable gradient and is limited to relatively small sweep angles and low Reynolds numbers.

Significantly more technology validation needs to be carried out before laminar flow can be incorporated into transport aircraft design. A better understanding of transition and how to predict it is also needed in order to design laminar-flow wings.

Determining boundary-layer transition location at conditions representative of transport aircraft has been largely limited to full-scale flight-testing. This is because the Reynolds numbers, model size needed, and low turbulence levels required restrict the use of wind tunnels. In addition, accurate predictions of the boundary-layer transition location from boundary-layer stability codes are difficult to obtain because these codes are still in the development and verification stage.

One earlier flight-test yielding encouraging results was a joint project of the NASA Ames Research Center's Dryden Flight Research Facility (Ames-Dryden) and NASA Langley Research Center. The experiment was flown on the F-111 transonic aircraft technology (TACT) aircraft. The TACT natural laminar flow (NLF) flight-test experiment (refs. 1–4) provided the first definitive flight results showing the effects of wing sweep on boundary-layer transition. The NLF experiment used a full-chord supercritical NLF airfoil. A section of the right wing panel of the F-111 TACT aircraft was covered with a glove having the NLF airfoil shape. This glove, made of foam and fiberglass, had a span of approximately 6 ft and a chord of 10 ft. The glove was designed to provide a favorable pressure gradient to approximately 70-percent chord.

Although somewhat limited, the F-111 TACT aircraft NLF results indicated that the adverse effect of leading-edge sweep was less than expected relative to earlier assumptions (ref. 1). In addition to providing transition data, the NLF experiment helped develop the construction techniques for making large contour modifications to metal wings from foam and fiberglass (ref. 8). Data from the F-111 TACT NLF flight experiment has also been used to enhance boundary-layer stability prediction methods (ref. 3).

Based on the favorable F-111 TACT aircraft NLF results, another flight experiment, the variable-sweep transition flight experiment (VSTFE) was initiated by NASA Langley and NASA Ames-Dryden. The VSTFE was initiated to help establish a boundary-layer transition database for use in laminar-flow wing design. The test facility for the VSTFE was an F-14A aircraft which had variable wing-sweep capability. The wing panels of the F-14A aircraft were modified with almost full-span, partial-chord gloves that had smooth surfaces suitable for natural laminar flow. The gloves could be constructed to change the wing airfoil shape if desired. These airfoil shapes could produce a wide range of pressure distributions for which transition location could be determined at various wing-sweep angles and flight conditions.

The three primary objectives of the F-14 VSTFE were as follows:

1. To determine the effects of wing sweep on laminar-to-turbulent boundary-layer transition at test conditions representative of transport aircraft with respect to Reynolds number, pressure distribution, noise, and cirrus clouds,

2. to establish a boundary-layer transition database for laminar-flow wing design and for evaluation of analytical techniques used for predicting the transition location, and

3. to determine transition location using several different measurement techniques and flow visualization techniques and compare the transition data obtained from each technique.

Two different gloves were flight-tested in the VSTFE: glove 1, a cleanup or smoothing of the basic F-14A wing, and glove 2, which was designed to provide specific pressure distributions at Mach number (M) 0.700 (refs. 9 and 10). The wing glove designs, flight-test techniques, and preliminary data are reported in references 11 through 13.

The F-14 VSTFE provided a large database of transition data for gloves 1 and 2. This paper describes the VSTFE and presents the glove 1 flight-test results, (VSTFE objectives 1 and 2). The transition techniques (objective 3) are discussed in reference 13.

NOMENCLATURE

AG	nondimensional chordwise location of the onset of the adverse gradient
BL	butt line location, in.
c	chord length, in.
cl	clean configuration of glove
C_p	coefficient of pressure, $(p - p_s)/\bar{q}$
dB	sound pressure level, decibels
hp	altitude, ft
M	freestream Mach number
NACA	National Advisory Committee for Aeronautics
NLF	natural laminar flow
p	local static pressure, lb/ft^2
p_s	freestream static pressure, lb/ft^2
p_t	total pressure, lb/ft^2
$\bar{q}$	dynamic pressure, lb/ft^2

Re_T	transition Reynolds number, Rnpu $\times x_T$
Rnpu	Reynolds number per unit foot, $\rho_\infty U_\infty / \mu_\infty$, 1/ft
TACT	transonic aircraft technology
T.P.	test point
U	local velocity, ft/sec
U/U_{max}	average maximum velocity at rake location, ft/sec
VSTFE	variable-sweep transition flight experiment
x	distance from glove leading edge, in.
x/c	ratio of distance from leading edge to local chord length
$(x/c)_T$	laminar-to-turbulent boundary-layer transition location
x_T	distance from glove leading edge to transition location, ft
Y	boundary-layer rake probe height, in.
α	angle of attack, deg
β	angle of sideslip, deg
δ	boundary-layer height, in.
$\delta*$	displacement thickness, $\int_0^\delta (1 - \rho U/\rho_{max} U_{max})\, dy$, in.
Λ	leading-edge wing sweep, deg
θ	momentum thickness, $\int_0^\delta (1 - \rho U/\rho_{max} U_{max})\, dy$, in.
ρ	density, slug/ft^3
μ	absolute viscosity, slug/ft-sec

Subscripts

T	transition location
∞	freestream

DESCRIPTION OF THE TEST AIRCRAFT CONFIGURATION

The following presents a description of the test vehicle used in the VSTFE and the natural laminar flow cleanup glove that was installed on the test vehicle for the glove 1 flight-tests.

F-14A Aircraft

An F-14A aircraft, equipped with two TF30-P414 engines, was the carrier vehicle for the VSTFE. The F-14A was chosen because it had variable-sweep wings (20 to 68°), favorable wing pressure distribution, suitable Mach and Reynolds number capability, and it was available for the experiment. The F-14A with glove 1 on the left wing is shown in figure 1.

For the flight-testing of glove 1, the upper surface of the left wing panel was cleaned up and smoothed by adding a constant-thickness glove made of foam and fiberglass. With the glove installed, the wing-sweep capability was restricted to a range of 20 to 35°, and the flaps and slats were locked in a retracted position.

Glove 1

Glove 1 was fabricated by applying a foam and fiberglass skin of essentially constant thickness over the existing skin of the F-14A wing section. The glove was initially 0.65-in. thick: 0.5-in. foam, six layers of fiberglass, and coated with a finish of polyester filler and paint. As illustrated in figure 2, the glove wrapped around the wing leading edge and extended back to the spoiler hinge line on the upper surface (~60-percent chord). The glove covered the majority of the wing span from butt line location (BL) stations 130 to 350, as shown in figure 1.

During the flight envelope verification phase of the experiment, small surface cracks developed in the glove. To repair these cracks, one additional layer of fiberglass was applied over the surface of the glove. The final glove included this additional layer of fiberglass and a finish of polyester body filler and paint, which added approximately 0.125 in. to the glove total thickness. The glove construction details, problems encountered, and solutions to the problems are discussed in reference 16.

The waviness of the glove surface was inspected and documented. Figure 3(a) presents surface waviness measurements for three wing stations on glove 1. These measurements were taken with the wing unloaded (zero load) and with the wing jacked from the lower surface to simulate a 1-*g* loaded condition, which was the condition for most of the flight tests.

The measurements were obtained with a mechanical deflection dial gauge having support feet 2 in. apart (fig. 3(b)). The dial gauge was attached to a wheel from which the distance along the glove surface could be determined. The outputs from both the dial gauge and the wheel were mechanically plotted when the unit was manually moved across the surface.

Because of the long chord lengths involved, two people were required to make the measurements. This caused an apparent roughness at the gauge handoff locations. The handoff locations are indicated in figure 3(a). In general, the glove is not as smooth in the simulated 1-*g* loaded condition as in the unloaded condition. However, even for this case, the maximum wave amplitudes were within 0.002 in/in, the criterion specified for glove construction.

INSTRUMENTATION

The instrumentation layout is shown in figure 4 and consisted of the following:

1. Three rows of flush static pressure orifices,
2. three rows of hot-film sensors,
3. two boundary-layer rakes,
4. three dynamic pressure transducers (microphones), and
5. three rows of surface pitot tubes.

In addition, liquid crystals were used for flow visualization at the middle station. The use of liquid crystals for flow visualization and interpretation of the data is described in references 11 and 13. The glove instrumentation systems were located in three test stations: inboard, between BL stations 160 and 204; middle, between BL stations 204 and 264; and outboard, between BL stations 264 and 324.

The following instrumentation systems were installed on the aircraft (at locations other than the wing glove):

1. A charge patch, installed on the left vertical tail,
2. an uplink guidance system, installed in the cockpit, and

3. a standard National Advisory Committee for Aeronautics (NACA) airdata noseboom.

All signals from the instruments were recorded on board the aircraft and most were downlinked to a ground station for real-time display and recording. The instrumentation systems, except the surface pitot tubes, are described in the following paragraphs. Surface pitot tube data were difficult to interpret and are not presented in this report. The surface pitot tube data are discussed in reference 13.

Flush Static Pressure Orifices

Flush static pressure orifices were created by drilling through the glove foam and fiberglass to 1-in. diameter cavities created by "target cups" which were glued to the wing surface and buried in the glove as described in reference 16. Each orifice had an inside diameter of 0.03 in. The individual target cups were connected to an electronic scanning pressure module with steel tubing. The maximum tube length was approximately 10 ft. Each orifice row consisted of 21 surface pressure orifices oriented streamwise to the airflow for a wing sweep of 20°. Table 1 presents the details of each orifice row.

Hot-Film Anemometer Systems

The hot-film system used constant temperature hot-film anemometers which are described in reference 13. The frequency modulation (FM) recorded hot-film data had a frequency response of 10 kHz. The hot-film sensors, as shown in figure 5, were mounted along a line oriented 30°-inboard relative to each orifice row, as indicated in figure 4. This was done to minimize any flow disturbance from one sensor affecting another. (The flow is turbulent after each sensor.) Each hot-film sensor was oriented streamwise to the flow for a wing sweep of 20°. Five hot-film sensors were operational for each flight. The location of the operational hot films varied from flight to flight as shown in table 2.

Boundary-Layer Rakes

Each boundary-layer rake consisted of 20 pitot pressure probes. To obtain more measurements close to the glove surface, the probes were mounted along a 4-in. slanted strut which was skewed 30° to the plane of the glove surface (fig. 6). With this type of rake orientation, the maximum probe distance from the glove surface was approximately 2.5 in. The rake probes were chamfered for less sensitivity to flow angularity. Each rake was oriented streamwise with the flow for a wing sweep of 20°. The pressures were measured with an electronic scanning pressure module. The maximum tube lengths were approximately 10 ft. The boundary-layer rake probe heights are presented in table 3.

Dynamic Pressure Transducers (Microphones)

Three dynamic pressure transducers (microphones) were used to survey the noise environment at the leading edge of the glove. The transducers were embedded flush to the glove surface. As shown in figure 4, there is one microphone for each test station located at approximately 3-percent chord, just inboard of each orifice row. The microphones were approximately 0.25 in. in diameter. The microphones at the inboard and outboard stations were located on the upper surface of the glove, and the middle section microphone was located on the lower surface of the glove. The output signal of each microphone was recorded on an onboard tape recorder and plotted after each flight. The frequency response of the FM recorded microphone data was 10 kHz. The microphones were positioned to be in laminar flow for most of the flight conditions.

Charge Patch

For the VSTFE program, a charge patch was used to detect the presence of ice particles or cirrus clouds. The charge patch was a 6-ft long portion of the left vertical tail shown in figure 7. The charge patch was, in an electronic sense, an isolated part of the airplane. The level of the charging current on the charge patch was monitored in real time and recorded during each flight.

The charge patch builds up a charge with the impact of particles, creating a current. The current created by the particles is measured in microamps, grows as a function of particle impacts, and dissipates as particle impacts cease. Changes in the current, not the magnitude of the current, are the prime indicators of encounters with particles. A detailed description of the charge patch can be found in reference 17.

Uplink Guidance System

The uplink is a flight trajectory guidance system which uses an analog cockpit display that indicates deviations from the desired flight conditions in real time. In the VSTFE, the uplink was used to obtain accurate flight conditions for each test point in a timely manner. The parameters used to guide the pilot were freestream Mach number (M), angle of attack (α), angle of sideslip (β), and altitude (hp). The uplink guidance system is discussed in detail in reference 18.

Aircraft Instrumentation

The airdata system, a standard NACA/NASA airdata head, was used to measure aircraft total and static pressures, angle of attack, and angle of sideslip. The total and static pressures were used to calculate parameters such as Mach number and dynamic pressure. Airspeed calibration data were obtained from a tower fly-by method and an acceleration–deceleration method (refs. 19 and 20). A complete description of the airdata system is found in reference 21. The angle of attack and sideslip flow direction vanes were mounted on the noseboom. Angle of attack was corrected for upwash and fuselage bending as described in reference 21.

Accuracy

The pressure range for the transducers was scaled for the desired flight conditions. The hot-film sensor and the microphone signals were calibrated and were responsive to a frequency well above 10 kHz, the frequency response of the FM tape recorder.

The estimated error in the flight measurements was as follows:

coefficient of pressure (C_p)	± 0.01
Mach number (M)	± 0.005
angle of attack (α)	$\pm 0.5°$
angle of sideslip (β)	$\pm 0.5°$
freestream static pressure (p_s)	± 0.7 lb/ft^2
total pressure (p_t)	± 0.7 lb/ft^2

FLIGHT-TEST CONDITIONS AND PROCEDURES

Glove 1 was tested at leading-edge sweep angles varying from 20 to 35°. Transition data at 15° of equivalent sweep were obtained by using a 5°-nose-right sideslip maneuver. The Reynolds number ranged from approximately

1×10^6 to 4×10^6/ft, which corresponds to minimum and maximum chord Reynolds numbers of 5×10^6 and 34×10^6, respectively. The conditions at which transition data were obtained are listed in table 4.

The glove 1 flight-test program was divided into two phases. The phase 1 flights were designed to clear an operating envelope and to calibrate the aircraft airspeed system. The operating envelope for the glove 1 flights is shown in figure 8. The maximum airspeed limit for the aircraft with the glove installed was 450 kn indicated airspeed or $M = 0.900$, whichever occurred first.

The laminar-flow data flights, phase 2, were conducted within the cleared envelope. Transition was determined using the previously described hot-film sensors and boundary-layer rakes.

Test conditions were selected to establish a database documenting the boundary-layer transition location as a function of angle of attack, Mach number, and Reynolds number (altitude). Maneuvers performed consisted primarily of trim points, level turns, and pushovers. Level turns were used to obtain data at greater than 1-g trim angles of attack, particularly at low altitudes (high dynamic pressures). Constant-g pushovers were used to obtain data at less than 1-g trim angles of attack.

Limited data were obtained at two additional test conditions. The first condition was flying with the left engine throttled back to examine the effects of engine noise on transition. The second test condition was flying through cirrus clouds to determine the effects of cirrus clouds on laminar flow.

Following each flight, the glove was inspected for surface cracks and insect impacts. The majority of the insect impacts occurred forward of 10-percent chord and, with very few exceptions, were not large enough to cause transition at the test altitudes. Although minor surface cracks were noted in the glove after the third flight, the glove surface remained within the established surface waviness tolerance. The conditions of the wing with respect to insect impacts, surface imperfections, and damage to the wing instrumentation were documented after each flight. The glove was cleaned and all necessary repairs to the glove instrumentation were made prior to each flight.

PRESENTATION OF RESULTS

Selected data are presented to illustrate the observed trends in the transition location (figs. 9 to 28). The flight conditions for these data are presented in the List of Figures. A microfiche supplement is provided which contains tabulated glove section pressure coefficients (table 5) and boundary-layer velocity profile (table 6) data. A tabulation of transition location obtained from the hot-film sensors for each test point is provided in table 7.

RESULTS AND DISCUSSION

The glove 1 transition results presented were primarily determined from hot-film sensors. Limited results from the boundary-layer rakes are also presented. The results include the effects of pressure distribution, angle of attack, Reynolds number, Mach number, engine noise, and cirrus clouds, in addition to the effects of wing sweep. Based on the analysis reported in reference 13, the hot-film and boundary-layer data were found to be the most repeatable. Thus results from the surface pitot tubes and flow visualization photos are not presented in this report.

Pressure Distributions

Figure 9 presents typical pressure distributions for the middle station at trim angles of attack and Mach numbers of 0.700 and 0.800. Although not shown, the pressure distributions for the inboard and outboard stations were similar.

The most notable characteristic is the change in leading-edge pressure gradient and pressure distribution shape with Mach number. At $M = 0.700$, the pressure distribution has a mildly favorable gradient that extends to about

0.3 x/c; the pressure distribution then becomes mildly adverse. At $M = 0.800$, the pressure distribution has a steep favorable gradient that extends to at least 0.5 x/c, where a normal shock occurs. One undesirable characteristic of the pressure distribution at $M = 0.700$ is the formation of an adverse pressure gradient (AG) near the leading edge for the two higher angles of attack shown in figure 9. This AG can preclude laminar flow aft of the leading-edge region. However, these undesirable characteristics in the pressure distribution were alleviated by decreasing the angle of attack. This is done by performing the pushover maneuver, mentioned earlier and described in reference 11.

Transition Data

Trends in the Transition Database

Presented in figure 10(a) is a graph of transition location and the beginning of the AG as a function of angle of attack for $\Lambda = 20°$, $M = 0.700$, and $hp = 35{,}000$ ft. Figures 10(b) and (c) provide pressure distributions for two discrete angles of attack. Data for all three stations are shown.

In figure 10(a) transition occurs aft of the AG, at all three stations except for one point at the inboard station. Below $\alpha = 2.0°$, the greatest difference between transition and the AG occurs at the middle station where AG occurs at 0.25 x/c and transition occurs at 0.40 x/c.

The corresponding pressure distribution in figure 10(b), $\alpha = 0.84°$, has a mildly favorable pressure gradient (negative slope, note sign convention) which gradually becomes unfavorable (positive slope) at all three stations. This trend is typical of the pressure distributions at $M = 0.700$. This gradual occurrence of the AG was always present in cases where transition occurred aft of the AG. This is an indication that laminar flow can be maintained in a small amount of AG.

Transition is observed to be moving forward as angle of attack increases in figure 10(a). This transition is a result of the leading-edge peak that occurs in the pressure distribution for the higher angle-of-attack values as shown in figure 10(c), for $\alpha = 3.4°$, and in figure 9. It is important to note that transition still occurs aft of the AG created by the leading-edge peak.

Another example of transition data at a condition with a mildly favorable pressure gradient, but for 35° of sweep, is shown in figure 11(a), for $M = 0.700$ and $hp = 35{,}000$ ft. For $\alpha < 2.0°$, transition at this condition occurs before the AG at all three stations, presumably because of crossflow disturbances. One exception which does occur at the AG is the maximum transition location, 0.35 x/c, occurring at the middle station. This is an encouraging laminar flow distance for 35° of leading-edge sweep.

The pressure distribution for a low angle of attack of 0.22°, (fig. 11(b)), has favorable pressure gradients to approximately 0.20–0.25 x/c at the inboard station, 0.25–0.30 x/c at the middle station, and 0.35–0.40 x/c at the outboard station. This type of mildly favorable or flat pressure distribution, shown in figure 11(b), resulted in the most aft transition location for the higher sweeps.

The AG remains constant at this condition to approximately $\alpha = 1.6°$, then moves forward with increasing angle of attack. An example of a pressure distribution for a higher angle of attack, 1.57°, is figure 11(c). Here the pressure coefficients near the leading edge have increased, resulting in a slight peak and relatively flat pressure gradients to approximately 0.25 x/c at all three stations.

Figure 12(a) is an example of transition data at a condition where the pressure distribution has a steep favorable pressure gradient. Figure 12(a) shows the transition location and AG as a function of angle of attack for $\Lambda = 20°$, $M = 0.800$, and $hp = 35{,}000$ ft. Pressure distributions at two discrete angle-of-attack values are shown in figures 12(b) and (c) for the same flight condition. Transition at this condition occurs very near (± 0.025 x/c) or forward of the AG. Transition at the inboard section occurs forward of the middle and outboard sections.

The pressure distributions shown in figures 12(b) and (c) have steep favorable gradients, which end abruptly with a normal shock. The exception to this is the inboard section pressure distribution at $\alpha = 1.46°$, figure 12(c), where the pressure gradient flattens out from 0.30 to 0.45 x/c before ending with a normal shock. These results are consistent trends in the transition database as a whole.

Maximum Transition Locations

Figures 13 through 17 present the most aft transition locations observed as a function of sweep for the inboard, middle, and outboard stations for all test conditions, except for stations where no transition data were obtained. These values were determined from the hot-film data exclusively. At conditions where the furthest forward hot-film sensor, 0.10 x/c, indicated turbulent flow transition was estimated to be at 0.05 x/c.

In figures 13 through 17 the transition location moves forward with increasing sweep in all cases. In addition, the effects of sweep on the forward movement of transition become more pronounced with increasing Mach number. As noted earlier, the pressure distributions have a very steep favorable gradient at $M = 0.800$, relative to $M = 0.700$. While for a given Mach number, the steep favorable pressure gradient delays the onset of transition at the lower sweep angles ($\leq 20°$); a steep pressure gradient can encourage transition at the higher sweep angles ($\geq 20°$). This is presumably because a steep pressure gradient increases the growth rate of cross flow disturbances resulting in the forward movement of the transition location.

At 35,000 ft, sweep angles of 30° and 35°, and $M = 0.700$, laminar flow was maintained to 0.4 x/c and 0.35 x/c respectively. With increasing Mach number, the most aft transition locations moved forward. This can be seen in figure 17. In addition to the higher unit Reynolds numbers at $M = 0.800$, one factor contributing to the forward movement of transition is the change in pressure distribution with increased Mach number.

In general, transition occurred earliest at the inboard station. This transition was expected since the inboard pressure distribution had a lower amount of chordwise favorable gradient relative to the middle and outboard station as shown in the pressure distribution portions of figures 10, 11, and 12. A comparison of figures 13 through 17 also shows transition moving aft with increasing altitude–decreasing Reynolds number, which is an expected result.

Maximum Transition Reynolds Number

Figure 18 presents the maximum transition Reynolds number as a function of sweep for $M = 0.700$, 0.750, and 0.800. At 30° and 35°, the most aft transition location and the greatest transition Reynolds numbers occurred at $M = 0.700$ (figs. 11 and 18). Transition at these conditions was generally presumed to be caused by cross flow disturbances, however, the furthest aft transition locations were caused by loss of a favorable pressure gradient. These transition results indicate that a pressure distribution with a mildly favorable pressure gradient, like those obtained at $M = 0.700$, are the most promising for laminar flow at sweeps above 20°.

The most aft transition location and maximum transition Reynolds number for 15 to 20° of sweep occurred at $M = 0.800$. Transition at these conditions was caused by the loss of favorable pressure gradient resulting from a normal shock. These transition results indicate that a pressure distribution with a steep favorable pressure gradient, like those obtained at $M = 0.800$, are the most promising for laminar flow at sweeps below 20°.

The maximum transition Reynolds number, 13.69×10^6, occurred at the middle station for $M = 0.800$, $hp =$ 20,000 ft, and an equivalent sweep of 15° (fig. 18). Table 8 presents the most aft transition obtained at each sweep angle and the flight conditions for which they occurred. Table 9 presents the maximum transition Reynolds number obtained at each sweep angle and the cause of transition.

Momentum Thickness Related to Skin Friction

Momentum thickness, θ, is directly related to skin friction and can be used as an indicator of the reduction in skin friction associated with maintaining an appreciable amount of laminar flow, that is, delaying transition to turbulent flow. Figures 19 through 21 present momentum thickness as a function of transition location at Mach numbers of 0.700 and 0.800 and sweeps of 20° and 35°. Assuming transition for a wing not designed for laminar flow occurs at 0.1 x/c, the maximum reduction in momentum thickness is approximately 58 percent. This can be noted in figures 19 through 22 as occurring at the outboard station for 20° of sweep, $M = 0.700$, and an altitude of 35,000 ft.

Two qualifying statements apply to the momentum thickness data presented. First, this experiment was not intended to be a complete airfoil test; only the forward 60-percent portion of the upper wing surface was gloved, and these results indicate an optimum reduction on the upper surface of only the middle and outboard stations. Second, these results were not all obtained at working lift coefficients; either a pushover or a windup turn maneuver was required to attain the conditions that would provide extensive laminar flow. However, there is no reason to expect that an airfoil contoured specifically for high-altitude lift coefficients could not attain comparable amounts of laminar flow at working or cruise lift coefficients.

Effects of Engine Noise on Transition

Noise levels for a sweep of 20°, trim angle of attack, and altitudes of 20,000 and 35,000 ft are presented in figures 22 and 23 for Mach numbers of 0.700 and 0.800 respectively. These noise levels are representative of those measured on the leading edge of the glove in a laminar-boundary layer. However, a leading-edge peak in the lower surface pressure distribution at lower angles of attack (that is, $\alpha < 0.5°$) may have caused turbulent flow at the middle microphone. These noise levels did not vary with sweep.

Noise levels for two engine conditions are compared in figure 24. The first condition was with the left engine at the normal throttle setting and the second was with the left engine throttled back. The figure is for $\Lambda = 30°$, $M \simeq 0.750$, and $hp = 35{,}000$ ft, at three different angle-of-attack values. Transition data at the middle station are shown for these tests on the middle station graphs.

Changes in the noise levels seen when the engine is throttled back are shown in figure 24. The most notable change is at the middle station where the noise level increases at the throttled-back engine setting. This increase in noise level may be caused by increased inlet noise which can occur when an engine is throttled back. The increase in noise level does change the transition location at the middle section. However, the change in transition was slight, ± 0.05 x/c, forward and aft with the engine throttled back and was not consistent with the engine throttle setting. Based on these typical results, the effects of engine noise on transition have been determined negligible.

Effects of Cirrus Clouds on Transition

A limited amount of data were obtained while the aircraft was flying through high-altitude cirrus clouds. Clouds typical of the type flown through are shown photographed from the ground in figure 25. Figure 26 shows hot-film and charge-patch signals without cloud encounters. Figures 28 and 29 show hot-film and charge-patch signals during cloud encounters.

Hot-film data obtained in clear skies are shown in figure 26(a). Each hot-film signal represents a different state of flow conditions from laminar to fully developed turbulent flow. The signals shown in figure 26(a) are used as a reference for comparison with the hot-film signals of figures 27 and 28. A detailed description on the method of interpretation of the hot-film signals is contained in reference 13.

A typical charge-patch signal is shown in figure 26(b). As previously discussed, the absolute magnitude of the signal is unimportant since the change in magnitude is the prime indicator of the presence of clouds. Figure 26(b) depicts a charge-patch output with no change in the magnitude, indicating no clouds.

Hot-film and charge-patch outputs obtained during a cloud encounter are presented in figure 27 for $\Lambda = 25°$, $M = 0.800$, and $hp = 35{,}000$ ft. Comparing the hot-film signals to the reference hot-film signals of figure 26(a), the 0.10, 0.20, 0.30, and 0.40 x/c signals appear mostly laminar (low-amplitude portions of signals) with turbulent bursts (high-amplitude spikes in signal). The amount of turbulent bursts increased as the hot-film location moved aft. Figure 28(b) shows the output of the charge patch for the same interval. The charge-patch signal shows several increases in amperage, indicating that particles were encountered. The turbulent bursts seen in the hot-film signals are presumed to be caused by the presence of clouds. Without the presence of clouds, transition occurred as far aft as 0.5 x/c, as indicated in figure 17.

The 0.5 x/c hot-film signal of figure 27(a) does not resemble any of the reference hot-film signals of figure 27. This signal has many high-amplitude spikes in an upward direction that would indicate laminar flow with turbulent spikes. However, there are a few downward spikes and areas where the signal indicates turbulent flow. Therefore, the 0.5 x/c signal is interpreted as being a turbulent signal with transition occurring between 0.4 and 0.5 x/c. The high-amplitude spikes in the upward direction indicate flow disturbances that may be attributed to the presence of clouds which have ice particles. This conclusion is confirmed by the charge-patch signal of figure 27(b).

Figure 28 presents data for $\Lambda = 25°$, $M = 0.790$, and $hp = 33{,}000$ ft during a cloud encounter where the cloud particles did not have an appreciable effect on the boundary-layer flow. The hot-film signals, shown in figure 28(a), do not exhibit interferences from cloud encounters as previously discussed. However, the corresponding charge-patch signal, figure 28(b) shows several areas of increased amperage indicating the presence of ice particles. Transition in this case is at approximately 0.4 x/c. These two examples are typical of the mixed results obtained in the cirrus cloud data. Based on these results, no conclusions were made regarding the effect of cirrus clouds on natural laminar flow in this experiment. A discussion of the effects of cirrus clouds on laminar flow is found in reference 17.

CONCLUDING REMARKS

The results of the F-14 variable-sweep transition flight experiment (VSTFE), glove 1 flight tests are presented herein. Transition location was determined as a function of wing sweep with respect to glove pressure distribution, Reynolds number, Mach number, and angle of attack. The transition data presented have been obtained primarily from hot-film sensors, with limited data also obtained from boundary-layer rakes. Limited data were obtained for evaluating the effects of engine noise and cirrus clouds on transition location. Transition data were obtained for leading-edge sweeps of 15 to 35°, Mach numbers ranging from 0.700 to 0.825, and altitudes ranging from 10,000 to 35,000 ft. The following summarizes the trends noted in the data.

The maximum transition Reynolds number obtained was 13.69×10^6 occurring at the middle test section for 15° of wing sweep, Mach number of 0.800, and an altitude of 20,000 ft.

The favorable pressure gradients for maintaining laminar flow ranged from steep at $M = 0.800$, to mildly favorable, at $M = 0.700$. The steep pressure gradient at $M = 0.800$ resulted in the furthest aft transition location for 15° and 20° of sweep, however this type of pressure gradient did not encourage laminar flow for sweeps of 25° and above. This trend was observed at all altitudes, despite the lower unit Reynolds numbers at 35,000 ft.

At an altitude of 35,000 ft, Mach number of 0.700, and 30° of sweep, laminar flow was maintained to 40-percent chord maximum and 35-percent chord maximum at 35° of sweep for the same flight conditions. These are encouraging results because sweep is believed to severely inhibit laminar flow.

At $M = 0.700$, transition tended to occur after the beginning of the AG. This is an indication that laminar flow can be maintained with a small, chordwise amount of AG.

As expected, transition moved aft with decreasing unit Reynolds number. Noise from the engines (based on changes in engine throttle setting) was not a significant factor affecting transition. Because of a limited amount of data obtained, no conclusions have been made regarding the effects of cirrus clouds in this experiment.

Ames Research Center
Dryden Flight Research Facility
National Aeronautics and Space Administration
Edwards, California, November 7, 1989

REFERENCES

1. Montoya, L.C., L.L. Steers, D.C. Christopher, and B.M. Trujillo, *F-111 TACT Natural Laminar Flow Glove Flight Results*, NASA CP-2208, 1981.

2. Meyer, Robert R., Jr., and Lisa A. Jennett, *In-flight Surface Oil-Flow Photographs With Comparisons to Pressure Distribution and Boundary-Layer Data*, NASA TP-2395, 1985.

3. Runyan, L. James, Brent H. Navran, and Rodger A. Rozendaal, *F-111 Natural Laminar Flow Glove Flight Test Data Analysis and Boundary-Layer Stability Analysis*, NASA CR-166051, 1984.

4. Boeing Commercial Airplane Company, *Natural Laminar Flow Airfoil Analysis and Studies*, NASA CR-159029, 1979.

5. Wagner, R.D., and M.C. Fischer, "Developments in the NASA Transport Aircraft Laminar Flow Program," AIAA-83-0090, Jan. 1983.

6. Rozendaal, Rodger A., *Natural Laminar Flow Flight Experiments on a Swept Wing Business Jet-Boundary-Layer Stability Analysis*, NASA CR-3975, 1986.

7. Runyan, L.J., G.W. Bielak, G.W., R. Behbehani, A.W. Chen, and R.A. Rozendaal, *757 NLF Glove Flight Test Results*, NLF and LFC Research Symposium, Langley Research Center, Hampton, VA, Mar. 16–19, 1987, NASA CP-2487, Part 3, pp. 795–818.

8. Bohn-Meyer, M., and Fred Jiran, "The Use of Techniques to Modify Airfoils and Fairings on Aircraft Using Foam and Fiberglass," AIAA-81-2445, Nov. 1981.

9. Rozendaal, Rodger A., *Variable-Sweep Transition Flight Experiment (VSTFE) Parametric Pressure Distribution Boundary-Layer Stability Study and Wing Glove Design Task*, NASA CR-3992, 1986.

10. Waggoner, E.G., R.L. Campbell, P.S. Phillips, and J.B. Hallissy, *Design and Test of an NLF Wing Glove for the Variable-Sweep Transition Flight Experiment*, NLF and LFC Research Symposium, Langley Research Center, Hampton, VA, Mar. 16–19, 1987, NASA CP-2487, Part 3, pp. 753–776.

11. Meyer, Robert R., Jr., Bianca M. Trujillo, and Dennis W. Bartlett, *F-14 VSTFE and Results of the Cleanup Flight Test Program*, NLF and LFC Research Symposium, Langley Research Center, Hampton, VA, Mar. 16–19, 1987, NASA CP-2487, Part 3, pp. 819–844.

12. Rozendaal, Rodger A., *Variable-Sweep Transition Flight Experiment (VSTFE) - Stability Code Development and Clean-Up Glove Data Analysis*, NLF and LFC Research Symposium, Langley Research Center, Hampton, VA, Mar. 16–19, 1987, NASA CP-2487, Part 3, pp. 845–860.

13. Anderson, Bianca Trujillo, Robert R. Meyer, Jr., and Harry R. Chiles, "Techniques Used in the F-14 Variable-Sweep Transition Flight Experiment," AIAA-88-2110, May 1988.

14. Moes, Timothy R., and Robert R. Meyer, Jr., *In-Flight Wing Pressure Distributions for the F-14A Aircraft*, NASA TM-85921, 1985.

15. Boppe, Charles W., and Bruce S. Rosen, *F-14 Aircraft High Speed Flow Simulations*, NASA CR-172559, 1985.

16. Bohn-Meyer, Marta M., "Constructing 'Gloved' Wings for Aerodynamic Studies," AIAA-88-2109, May 1988.

17. Davis, Richard E., Dal V. Maddalon, and Richard D. Wagner, *Performance of Laminar-Flow Leading-Edge Test Articles in Cloud Encounters*, NLF and LFC Research Symposium, Langley Research Center, Hampton, VA, Mar. 16–19, 1987, NASA CP-2487, Part 3, pp. 163–194.

18. Meyer, R.R., Jr., and Cdr. E.T. Schneider, "Real-Time Pilot Guidance System for Improved Flight-Test Maneuvers," AIAA-83-2747, Nov. 1983.

19. Johnson, J. Blair, Terry J. Larson, and Jules M. Ficke, *Digital Program for Calculating Static Pressure Position Error*, NASA TM-86726, 1987.

20. Sakamoto, G. M., *Aerodynamic Characteristics of a Vane Flow Angularity Sensor System Capable of Measuring Flightpath Accelerations for the Mach Number Range from 0.4 to 2.54*, NASA TN D-8242, 1976.

21. DeAnda, Albert G., *AFFTC Standard Airspeed Calibration Procedures*, AFFTC-TIH-81-5, June 1981.

Table 1. Surface pressure orifice locations.

Location	BL station, in.	Chord, in.	Chord, percent
Inboard	200.9	103.7	
Middle	260.0	84.8	
Outboard	320.0	65.4	
Upper surface			0.0, 0.5, 1.0, 2.0, 4.0, 6.0, 8.0, 10.0, 12.0, 15.0, 17.0, 20.0, 25.0, 30.0, 35.0, 40.0, 45.0, 50.0, 55.0
Lower surface			0.5, 1.0

Table 2. Hot-film gage locations, percent chord.

Flight	Inboard, (BL 162–196 in.)	Middle, (BL 228–256 in.)	Outboard, (BL 294–316 in.)
12	No hot-film gages	No hot-film gages	10.8, 15.0, 20.0, 30.0, 40.8
13	↓	No hot-film gages	10.8, 20.0, 30.0, 40.8, 50.0
15–21	↓	11.1, 20.0, 30.0, 40.0, 50.0	No hot-film gages
22–25	11.3, 20, 30, 41.3, 50.0	No hot-film gages	↓
25–30	No hot-film gages	11.3, 20.0, 30.0, 41.3, 50.0	↓
31	↓	Gain of 8 on hot-film gages	↓
32	↓	Gain of 25 on hot-film gages	↓
33	↓	↓	↓
34, 35	↓	No hot-film gages	10.0, 20.0, 30.0, 40.0, 50.0

Table 3. Boundary-layer rake locations.

Locations	Rake 1	Rake 2
BL station, in.	230	290
Chord, percent	55.0	55.0
Rake probe heights, in.	0.03	0.04
	0.05	0.07
	0.11	0.12
	0.17	0.18
	0.22	0.21
	0.27	0.27
	0.32	0.31
	0.36	0.37
	0.41	0.42
	0.51	0.53
	0.72	0.73
	0.91	0.94
	1.11	1.15
	1.30	1.35
	1.53	1.55
	1.74	1.75
	1.95	1.95
	2.14	2.16
	2.35	2.37
	2.55	2.58

Table 4. Test conditions.

Sweep, deg	Sideslip, deg
20	0, −5, +5
25	0
30	0
35	0

M = 0.700, 0.750, 0.800, 0.825

hp = 10,000, 20,000, 25,000, 30,000, 35,000

α = 0° to 5°

Table 5. Glove section pressure coefficients.
Microfiche pages m-1 through m-1114.

Table 6. Boundary-layer velocity profile data.
Microfiche pages m-1115 through m-2260.

Table 7. Boundary-layer transition locations.
Microfiche pages m-2261 through m-2288.

Tables 5–7 are in the microfiche supplement included with this report and are also available on disk from the author upon request.

Table 8. Maximum transition location for each sweep angle, middle station.

Leading-edge wing sweep, deg	$(x/c)_T$	Mach number	Altitude, ft	Apparent cause of transition
15	0.55	0.800	20,000 25,000	Loss of favorable pressure gradient due to normal shock
20	0.525	0.800	30,000 35,000	Loss of favorable pressure gradient due to normal shock
25	0.50	0.800	35,000	Loss of favorable pressure gradient due to normal shock
30	0.40	0.700	35,000	Loss of favorable pressure gradient
35	0.35	0.700	35,000	Loss of favorable pressure gradient

Table 9. Maximum transition Reynolds number for each sweep angle, middle station.

Leading-edge wing sweep, deg	Transition Reynolds number $\times 10^6$	Mach number	Altitude ft	Apparent cause of transition
15	13.69	0.800	20,000	Loss of favorable pressure gradient due to normal shock
20	10.95	0.800	25,000	Loss of favorable pressure gradient due to normal shock
25	7.82	0.800	35,000	Loss of favorable pressure gradient due to normal shock
30	5.23	0.700	35,000	Loss of favorable pressure gradient
35	4.54	0.700	35,000	Loss of favorable pressure gradient

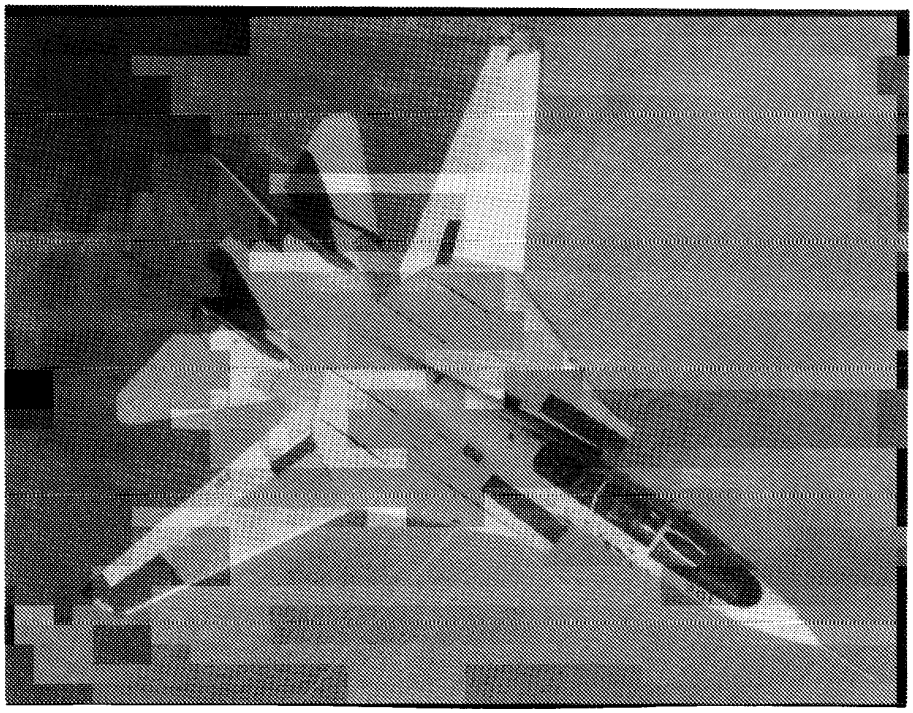

EC 86-33403-001

Figure 1. F-14A aircraft with glove 1 on left wing.

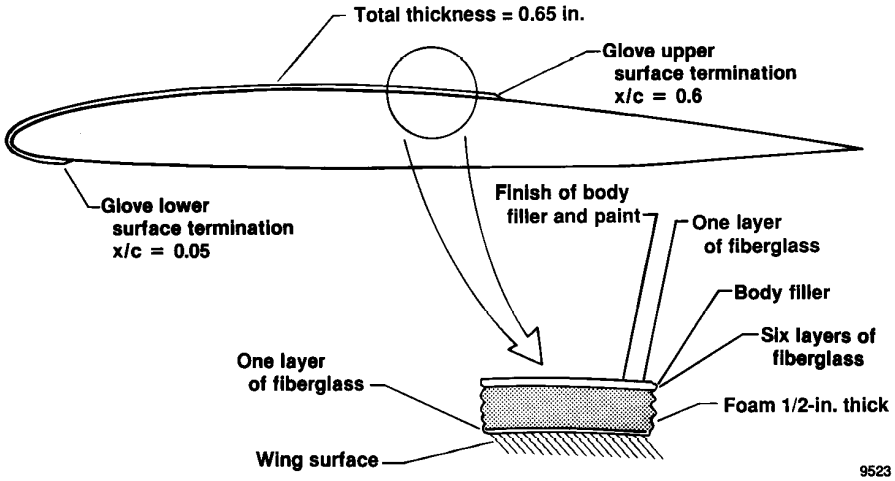

Figure 2. Typical glove 1 cross section.

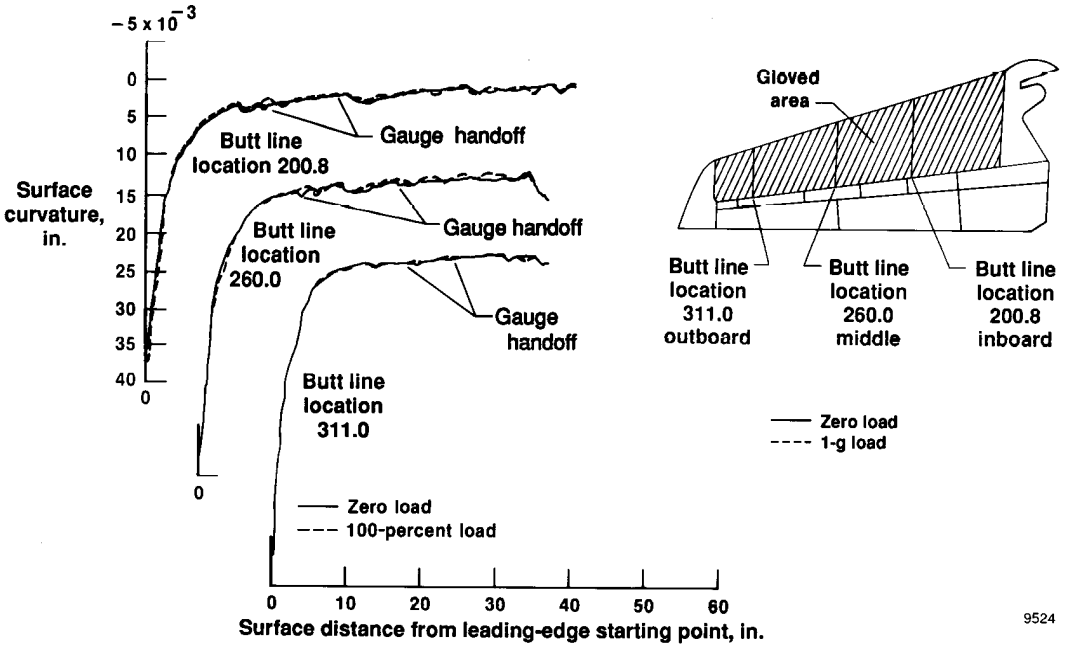

(a) Waviness measurements.

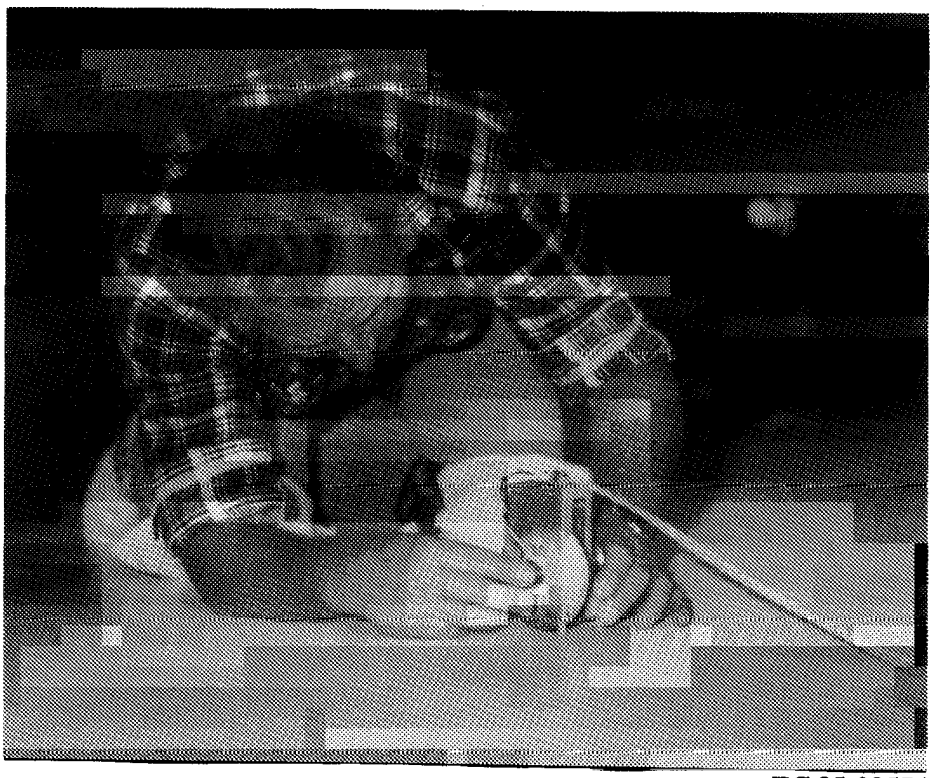

EC 85-32574

(b) Mechanical deflection dial gauge used to measure glove surface curvature.

Figure 3. Glove 1 waviness.

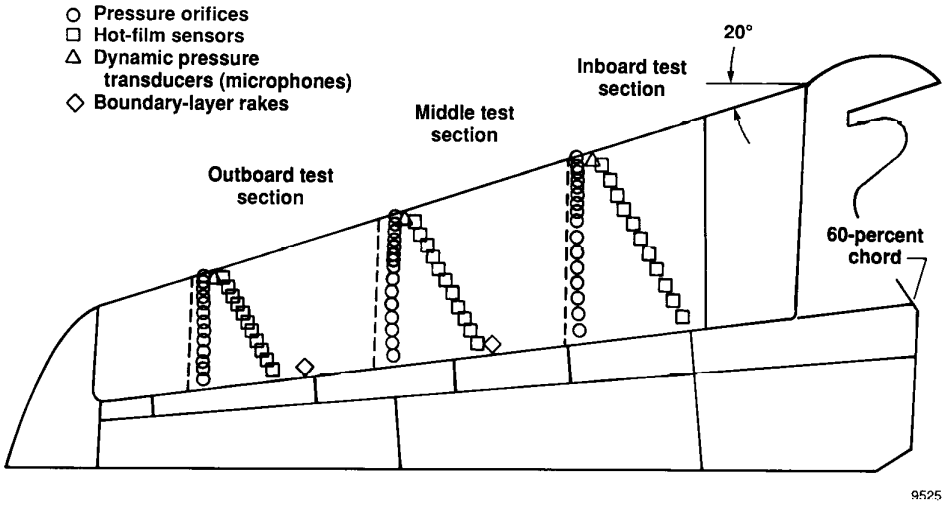

Figure 4. Glove 1 upper surface planform and instrumentation layout.

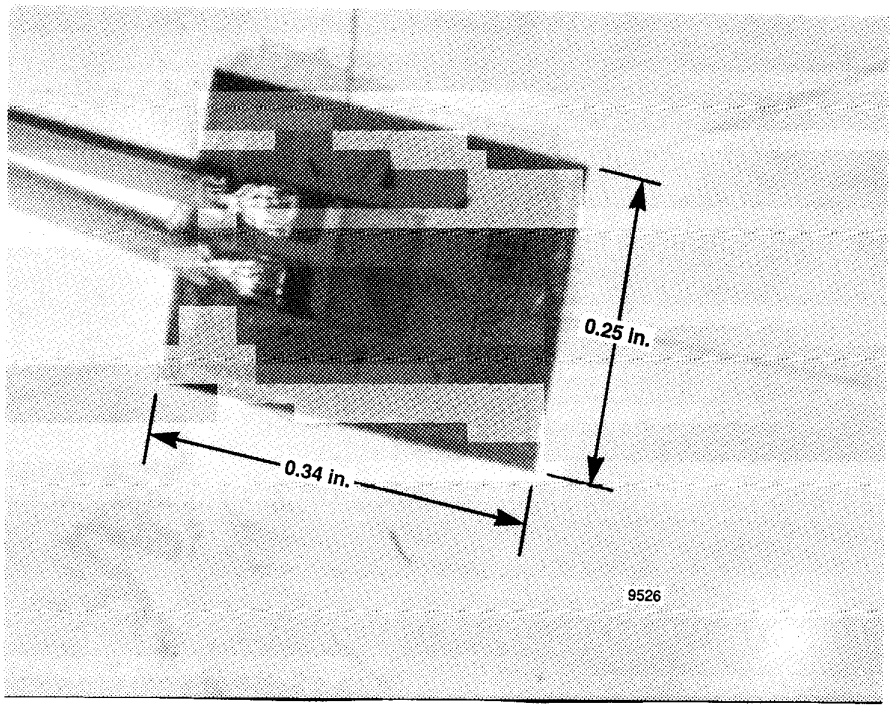

Figure 5. Glove 1 hot-film sensor.

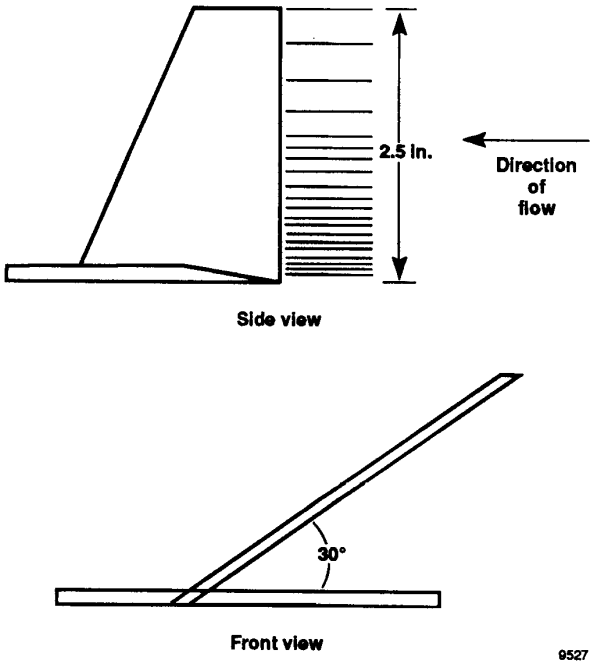

Figure 6. Boundary-layer rake.

ECN 86-33481-002

Figure 7. Charge-patch location.

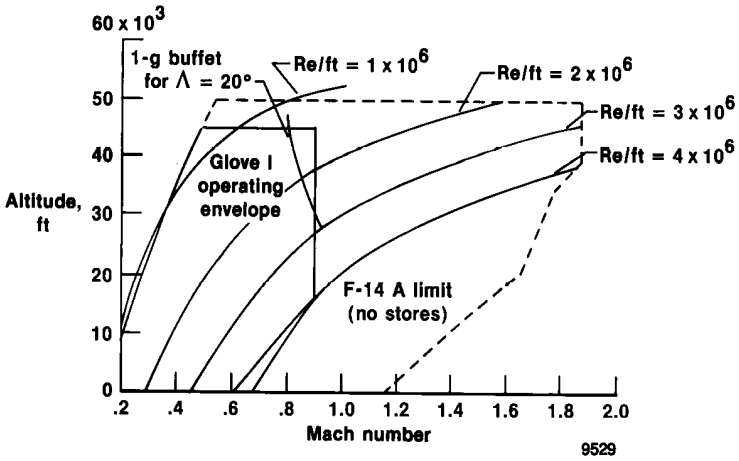

Figure 8. Glove 1 operating envelope.

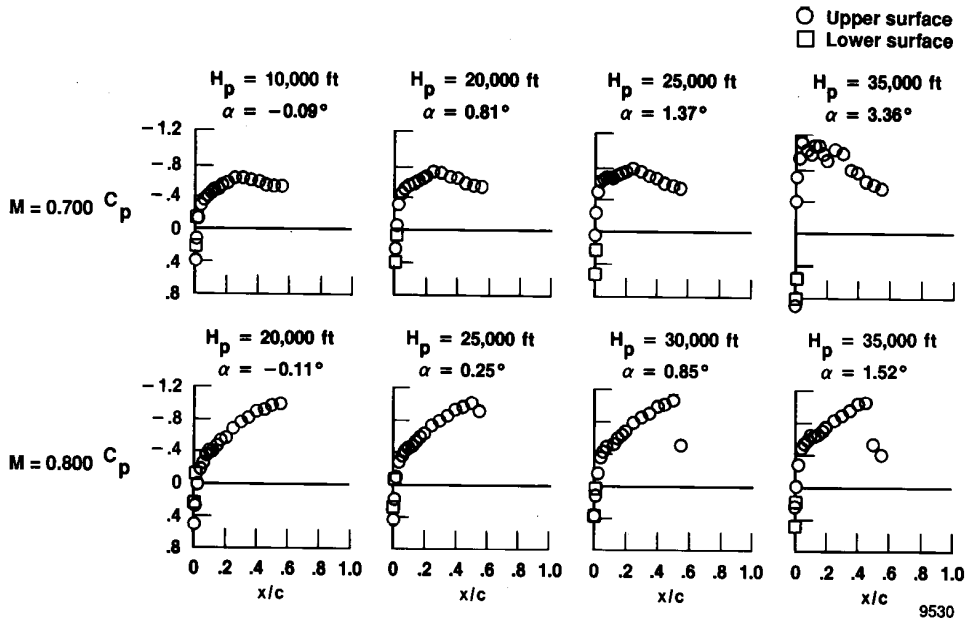

Figure 9. Glove 1 middle station pressure distributions; α = trim, Λ = 20°.

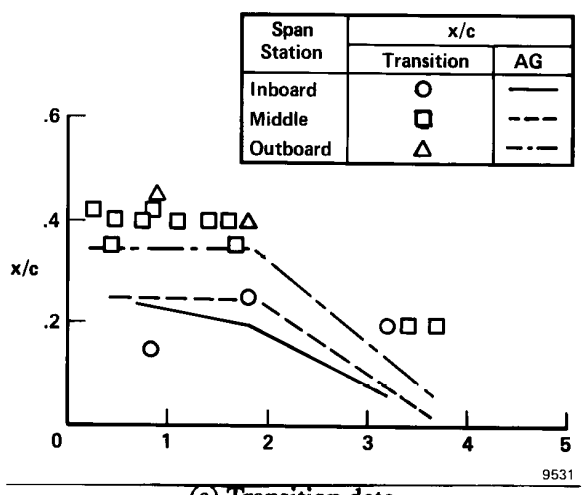

(a) Transition data.

Figure 10. Transition data and pressure distributions for M = 0.700, Λ = 20°, and hp = 35,000 ft.

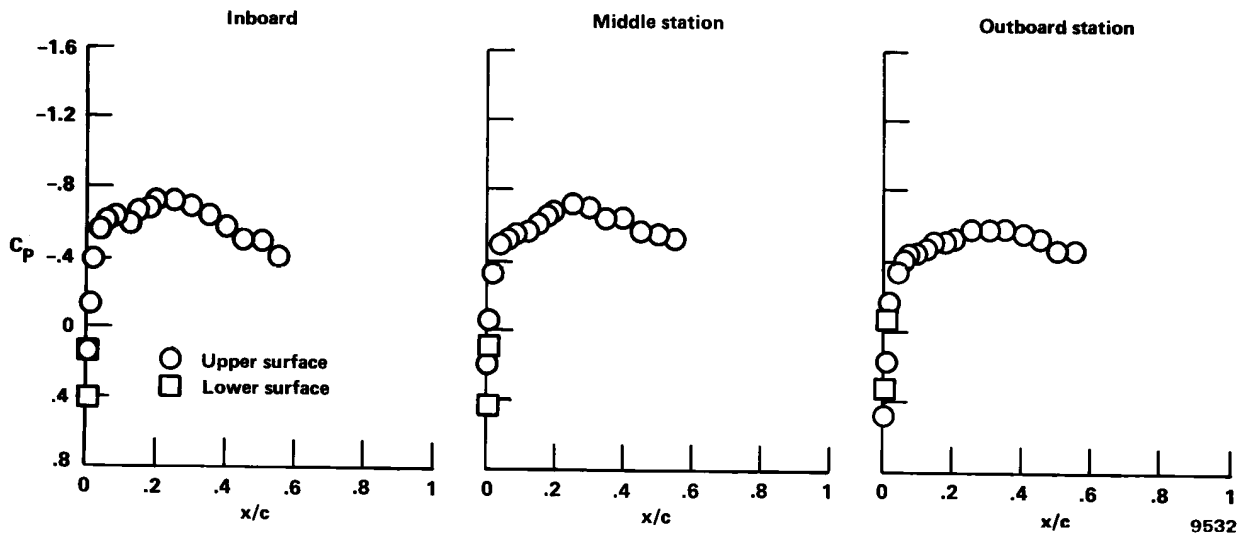

(b) Pressure distributions, $\alpha = 0.84°$.

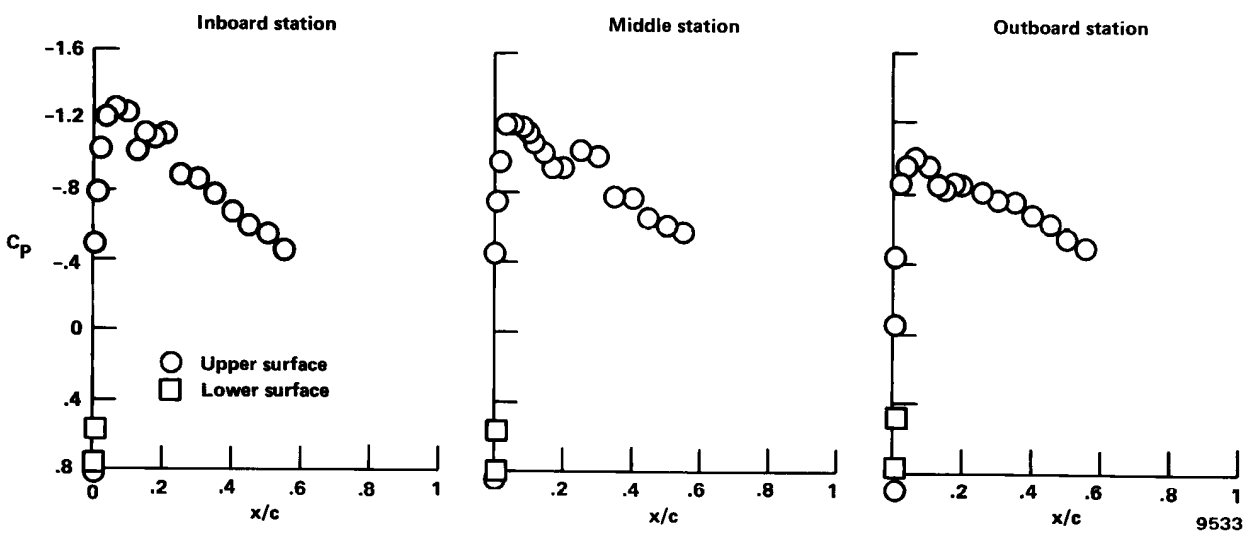

(c) Pressure distributions, $\alpha = 3.4°$.

Figure 10. Concluded.

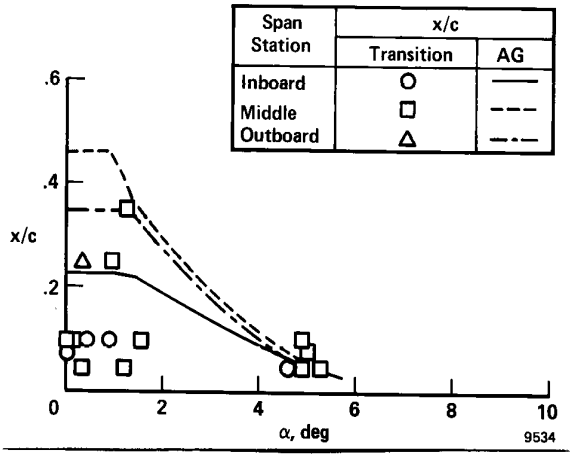

(a) Transition data.

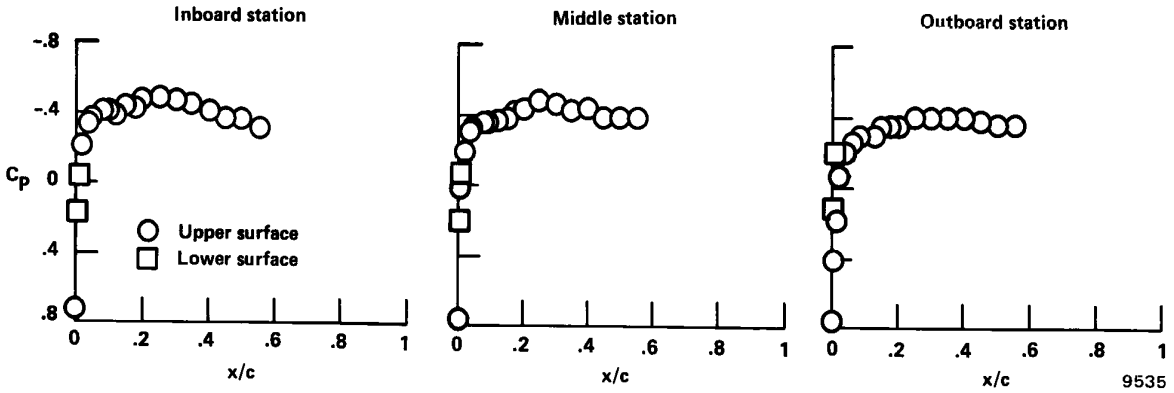

(b) Pressure distributions, $\alpha = 0.22°$.

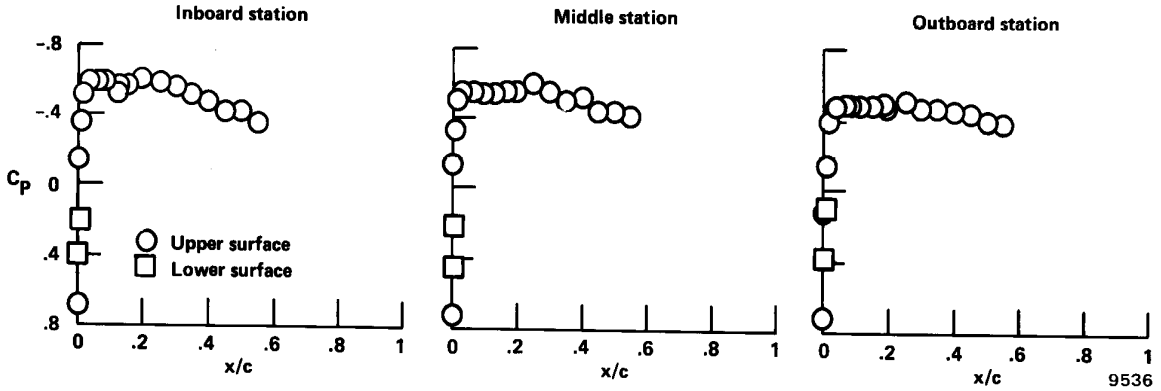

(c) Pressure distributions, $\alpha = 1.57°$.

Figure 11. Transition data and pressure distributions for $M = 0.700$, $\Lambda = 35°$, and $h_p = 35{,}000$ ft.

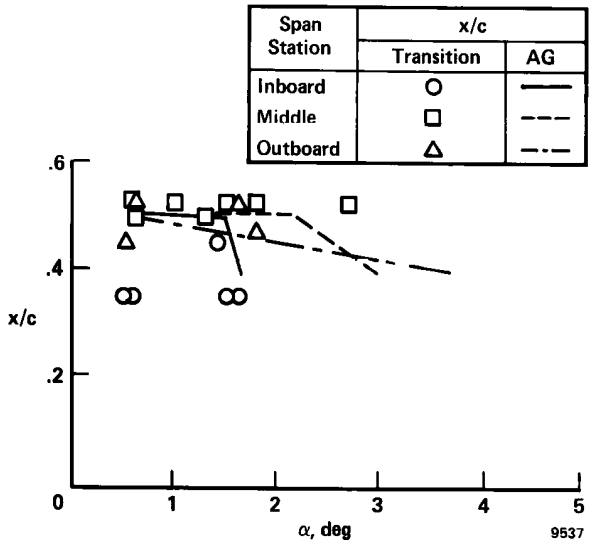

(a) Transition data.

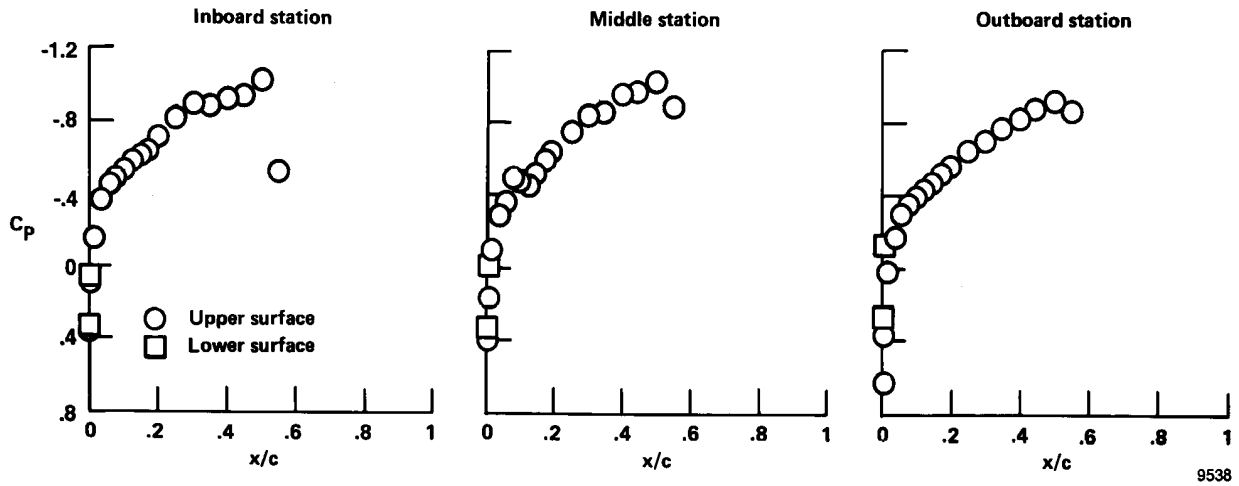

(b) Pressure distributions, $\alpha = 0.46°$.

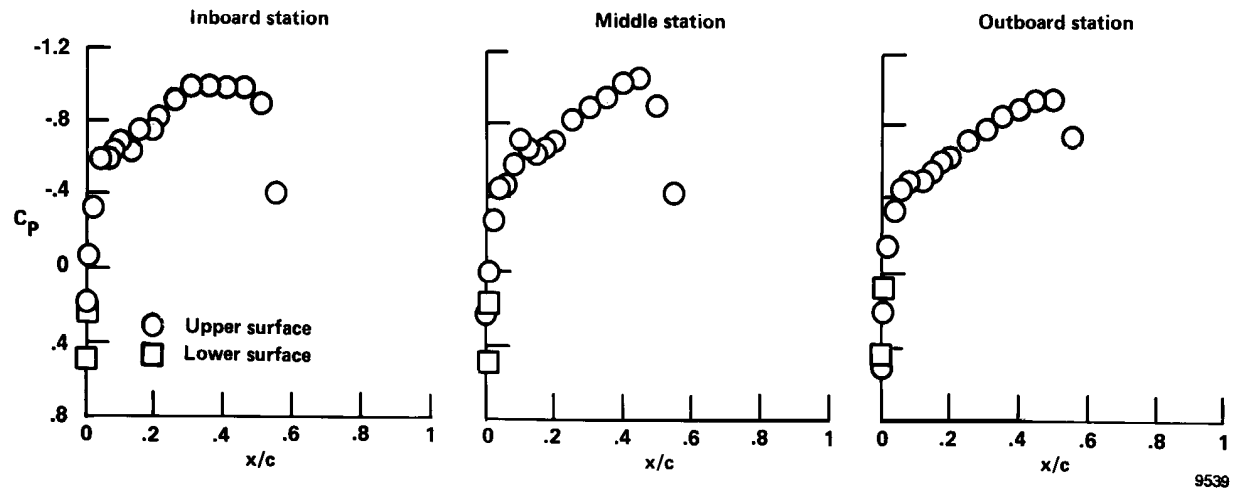

(c) Pressure distributions, $\alpha = 1.46°$.

Figure 12. Transition data and pressure distributions for $M = 0.800$, $\Lambda = 20°$, and $hp = 35{,}000$ ft.

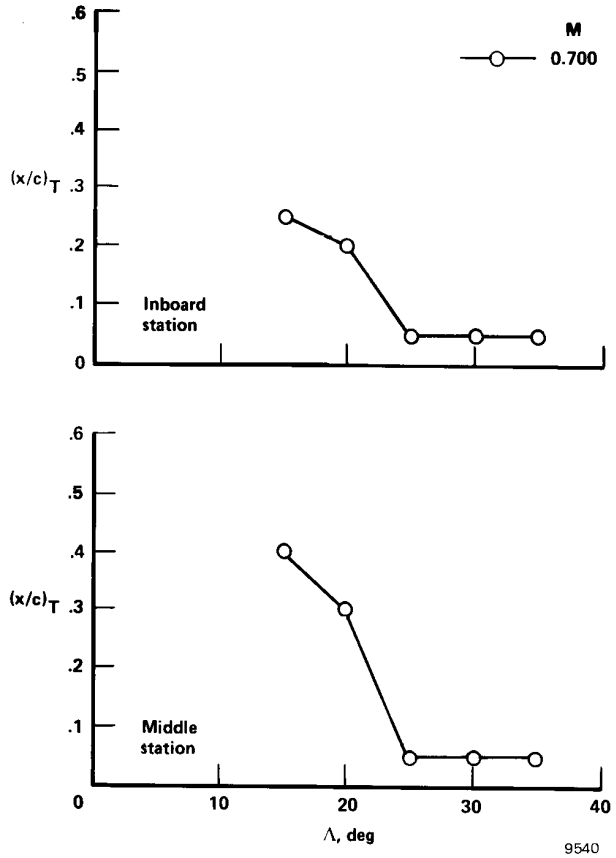

Figure 13. Maximum transition location as a function of sweep; $M = 0.700$, $hp = 10{,}000$ ft.

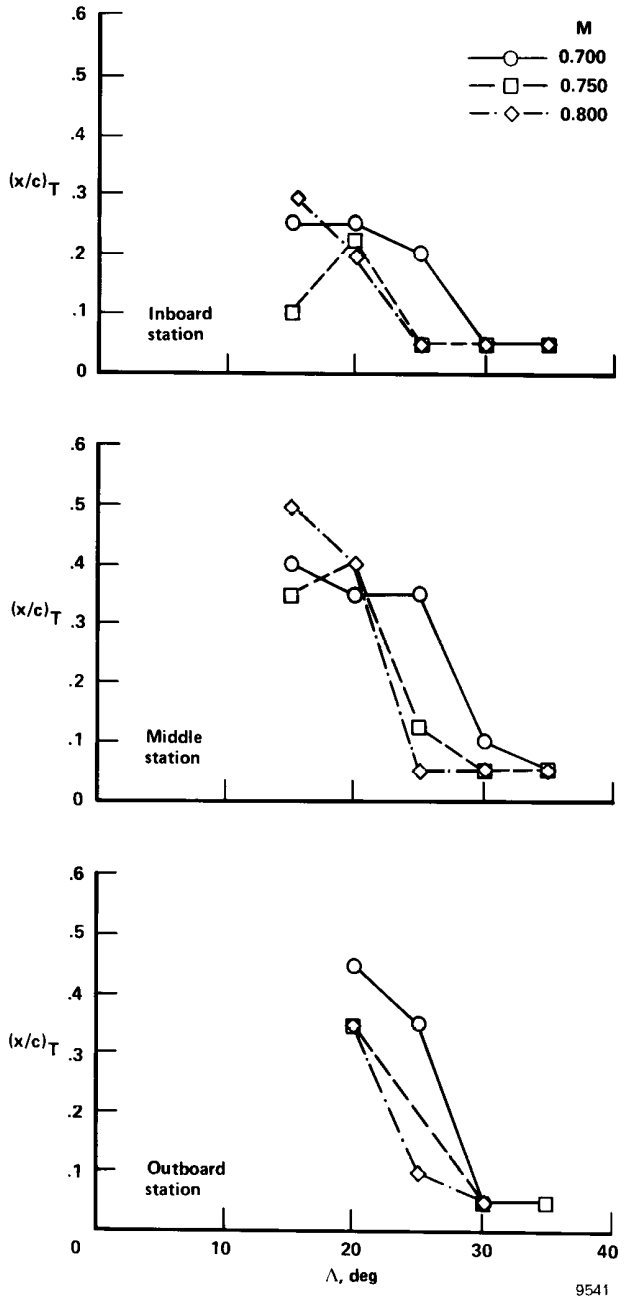

Figure 14. Maximum transition location as a function of sweep; M = 0.700, 0.750, 0.800 and hp = 20,000 ft.

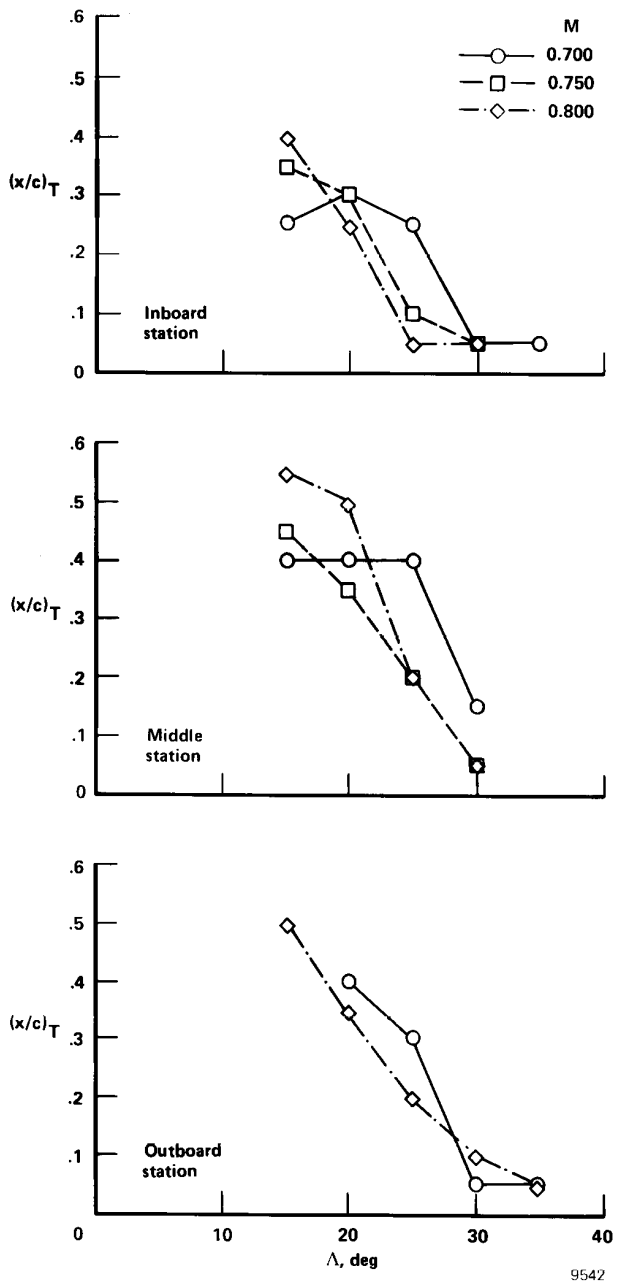

Figure 15. Maximum transition location as a function of sweep; $M = 0.700, 0.750, 0.800$ and $hp = 25{,}000$ ft.

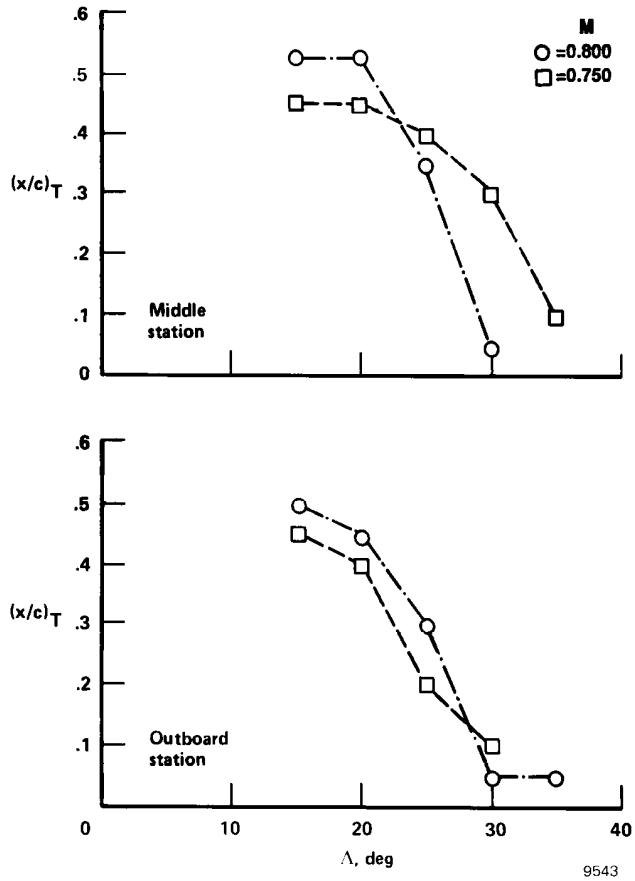

Figure 16. Maximum transition location as a function of sweep; M = 0.750, 0.800 and hp = 30,000 ft.

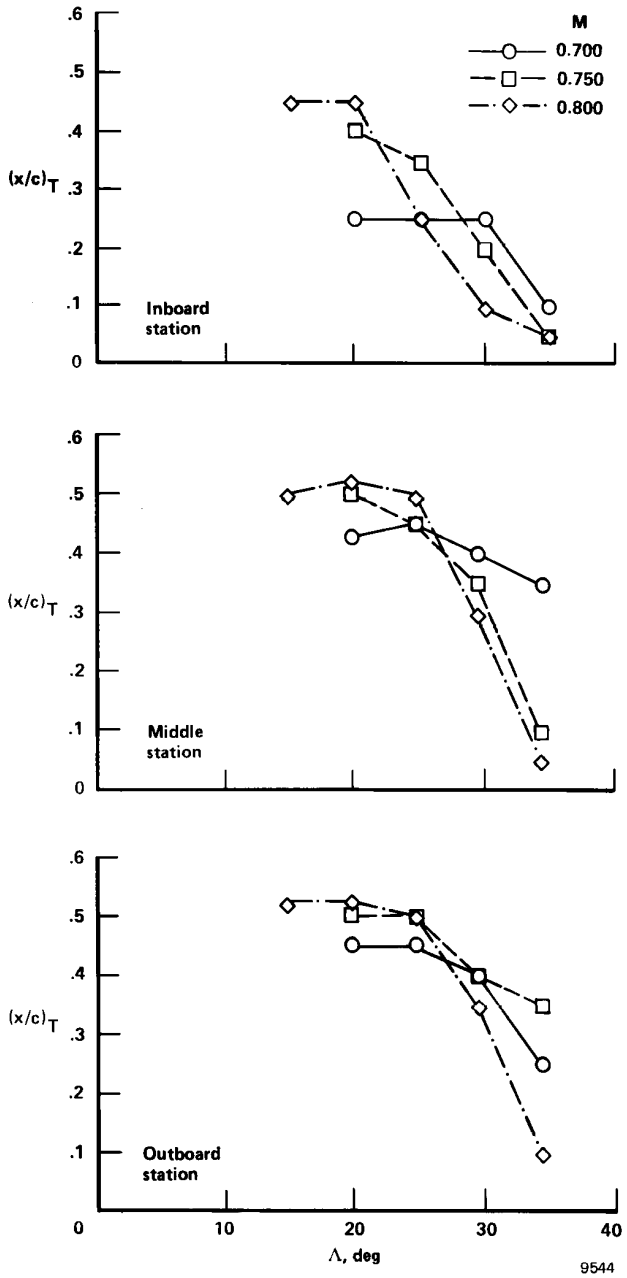

Figure 17. Maximum transition location as a function of sweep; M = 0.700, 0.750, 0.800 and hp = 35,000 ft.

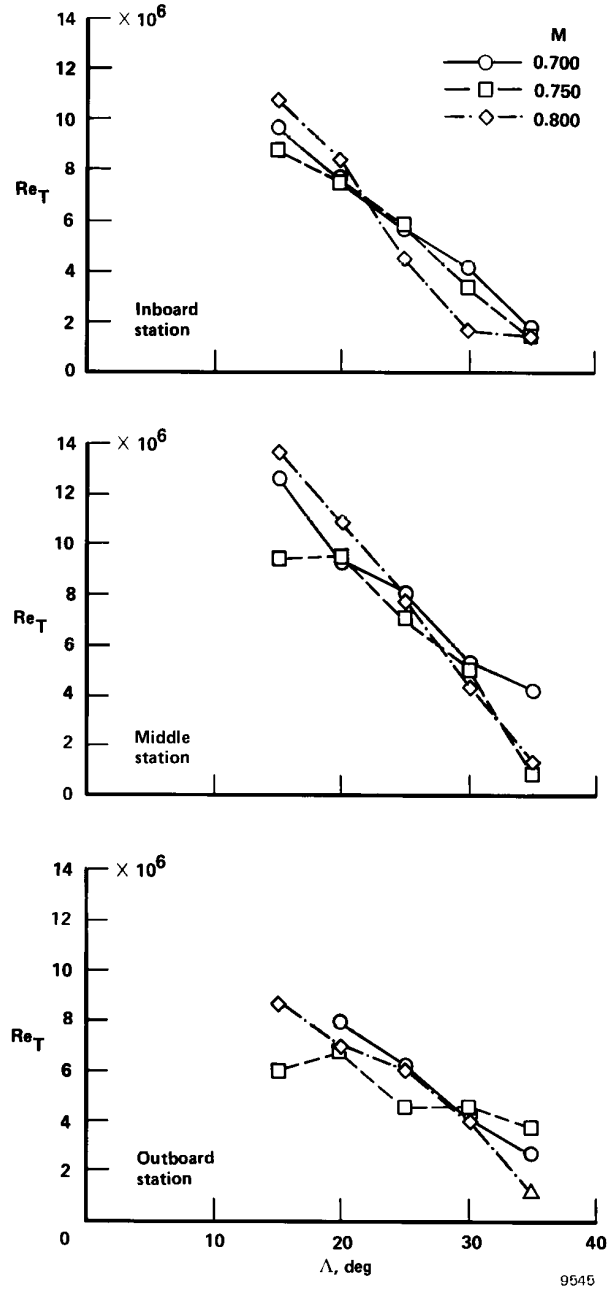

Figure 18. Maximum transition Reynolds number as a function of sweep.

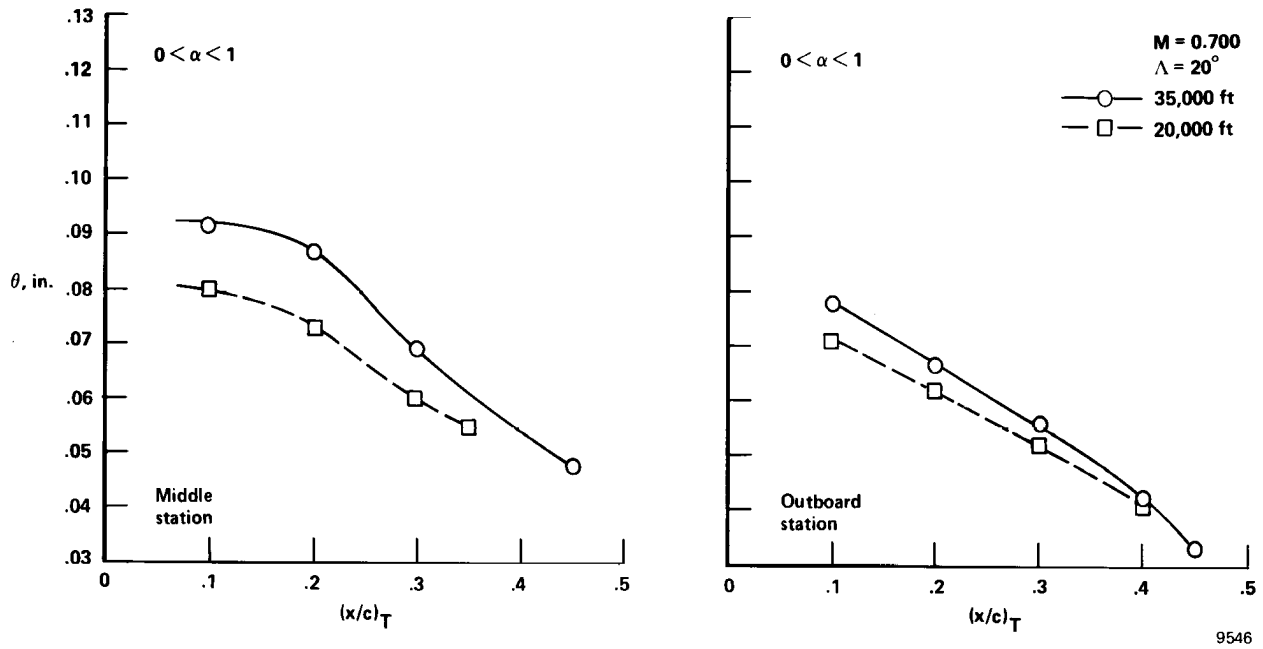

Figure 19. Momentum thickness as a function of transition location for $M = 0.700$, $\Lambda = 20°$, and $hp = 20{,}000$ and 35,000 ft.

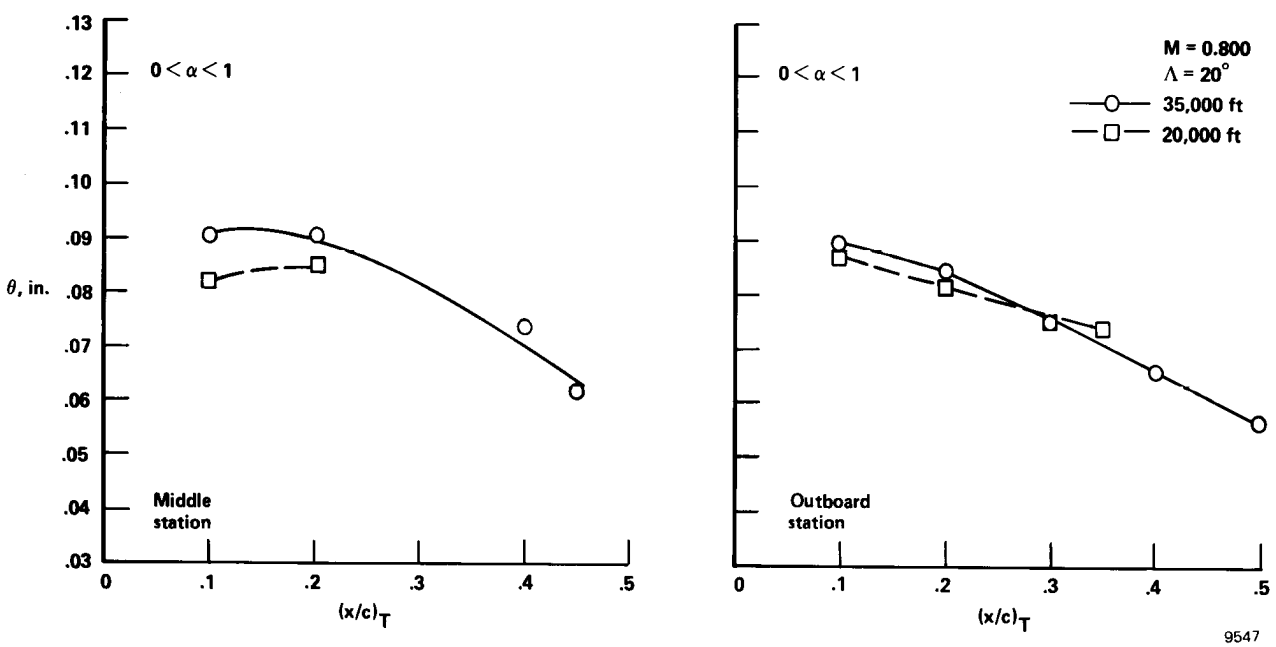

Figure 20. Momentum thickness as a function of $(x/c)_T$, $M = 0.800$, and $\Lambda = 20°$.

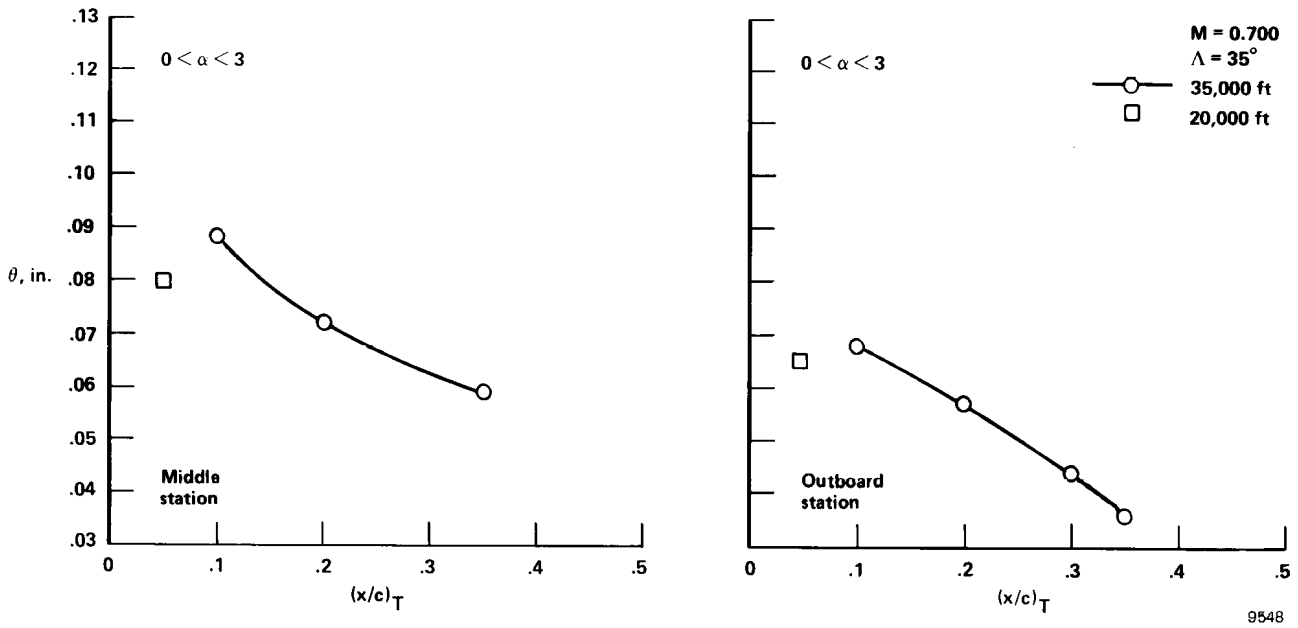

Figure 21. Momentum thickness as a function of $(x/c)_T$, $M = 0.700$, and $\Lambda = 35°$.

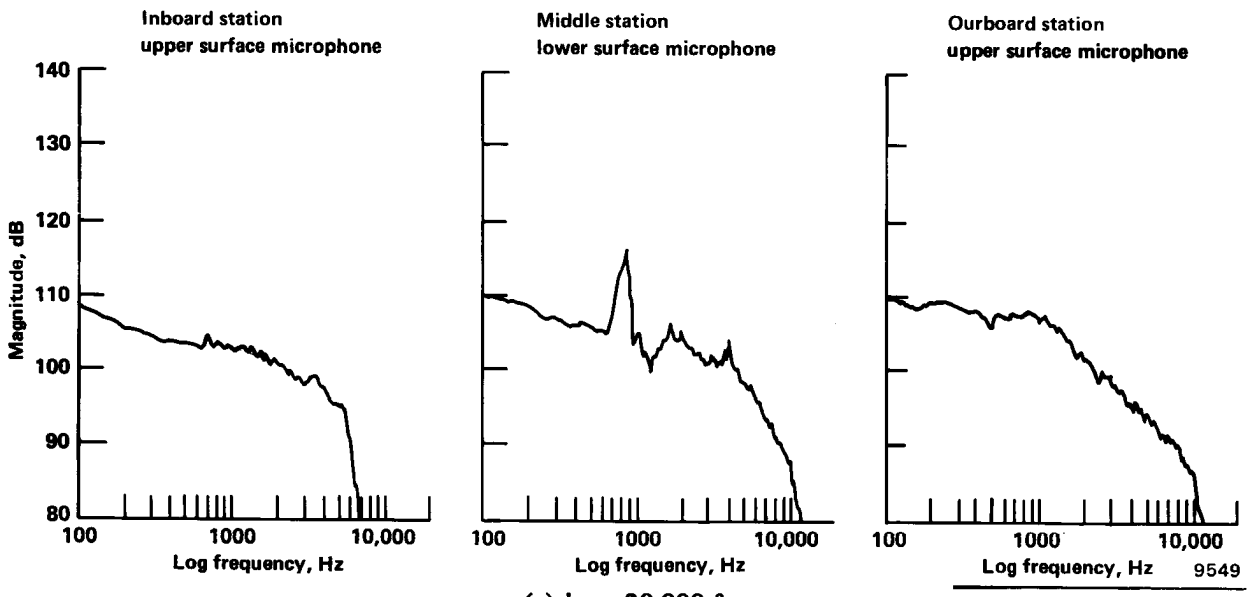

(a) $hp = 20{,}000$ ft.

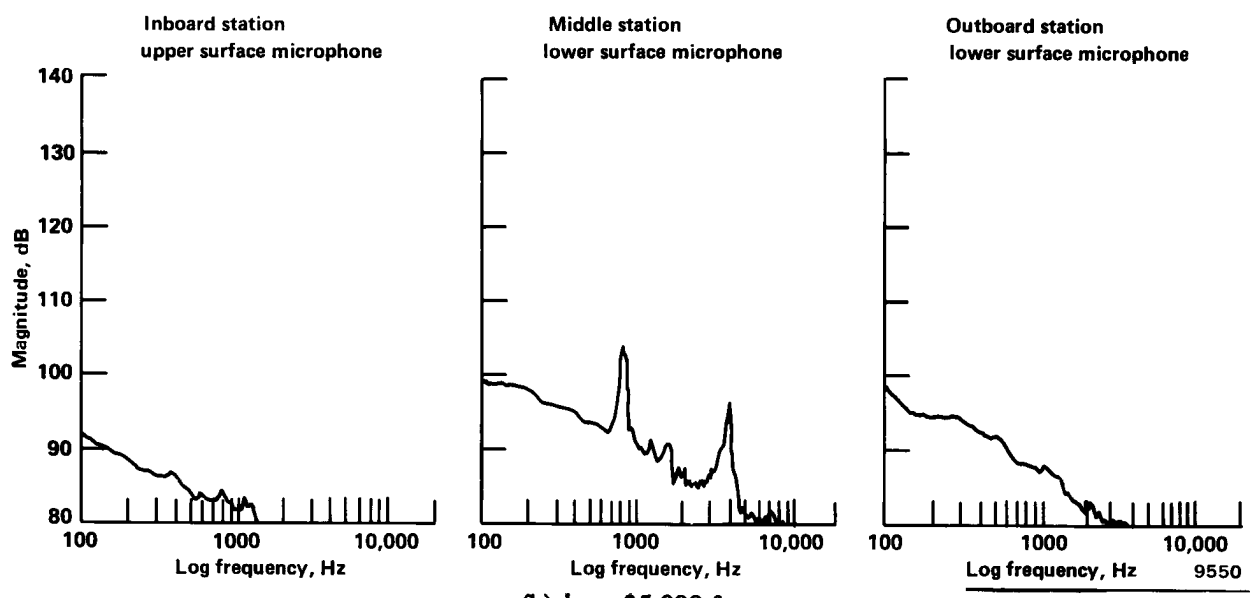

(b) $hp = 35{,}000$ ft.

Figure 22. Microphone data for $M = 0.700$ and $\Lambda = 20°$.

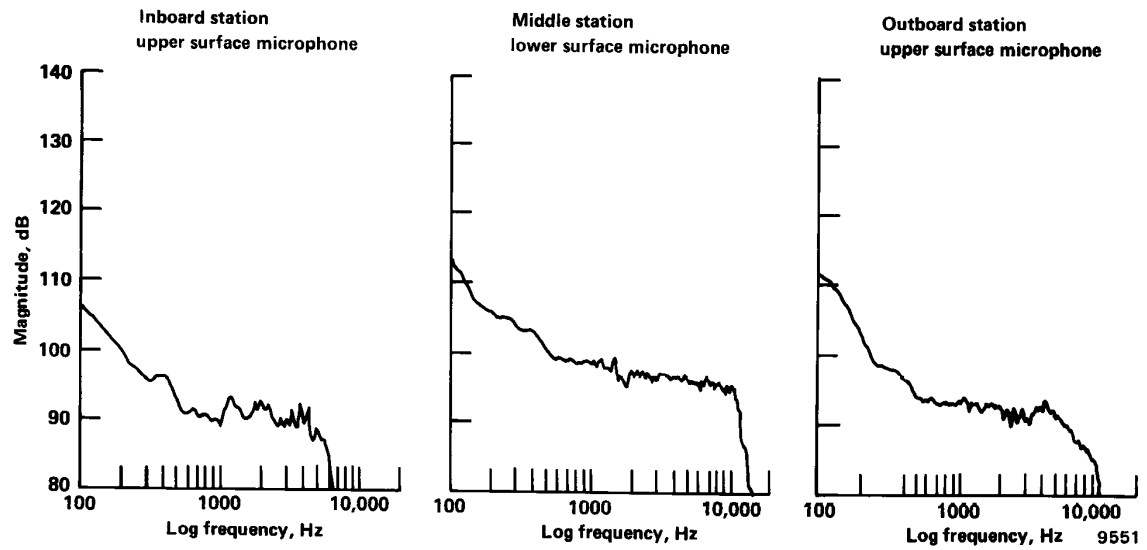

(a) $hp = 20{,}000$ ft.

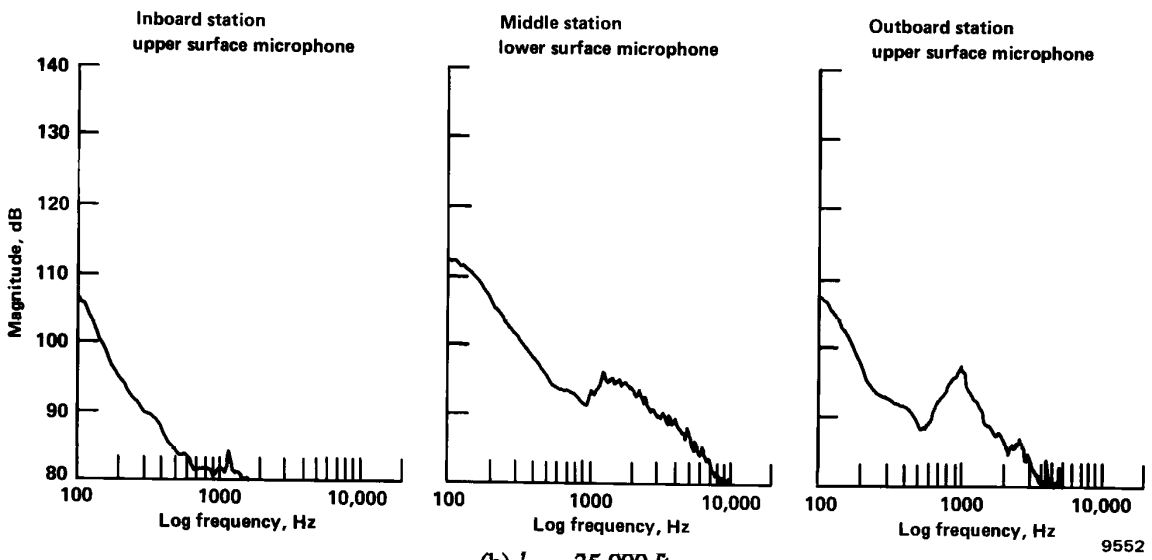

(b) $hp = 35{,}000$ ft.

Figure 23. Microphone data for $M = 0.800$ and $\Lambda = 20°$.

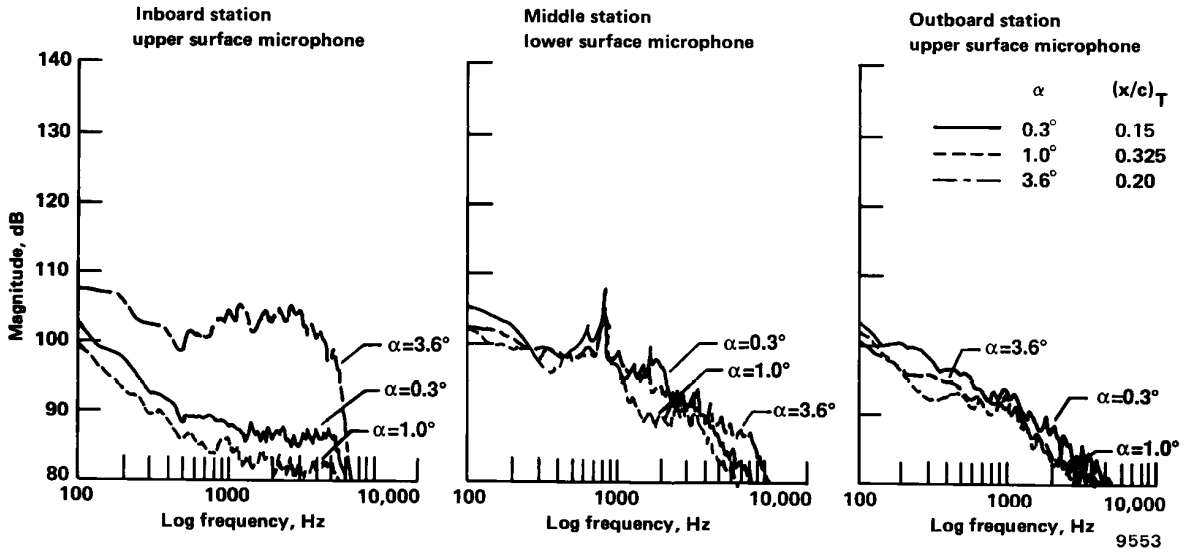

(a) Normal throttle setting.

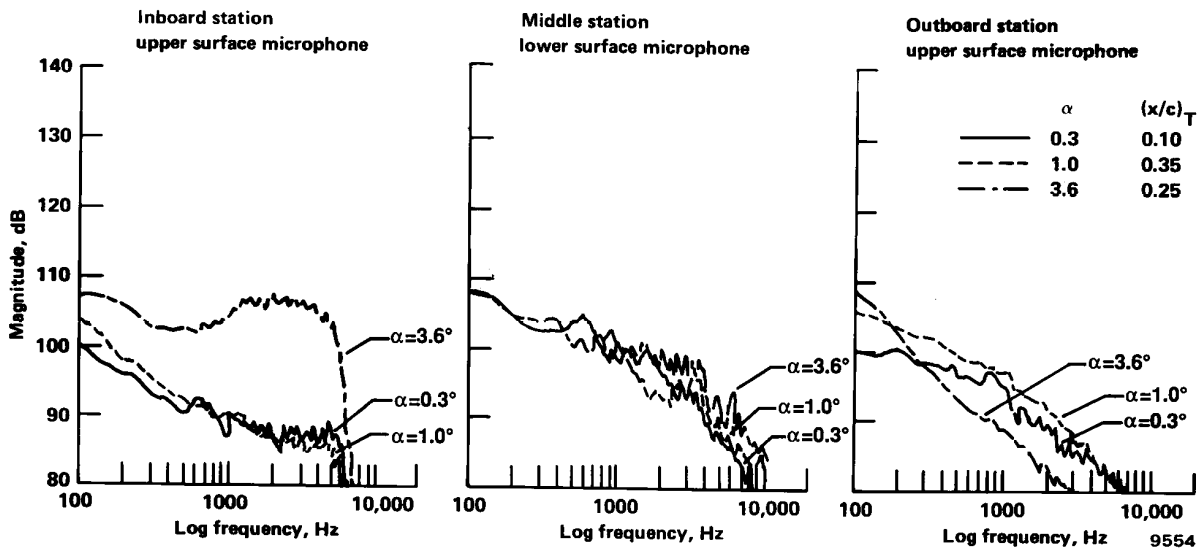

(b) Left engine throttled back.

Figure 24. Microphone data for leading-edge noise study; $M = 0.750$, $\Lambda = 30°$, and $hp = 35{,}000$ ft.

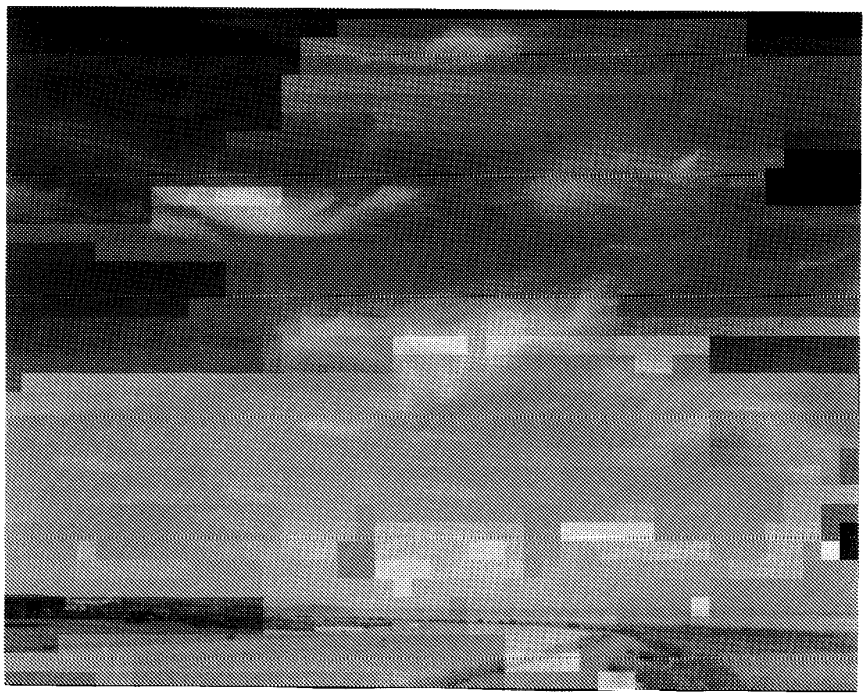

EC 86-33533-001

Figure 25. Typical cirrus clouds.

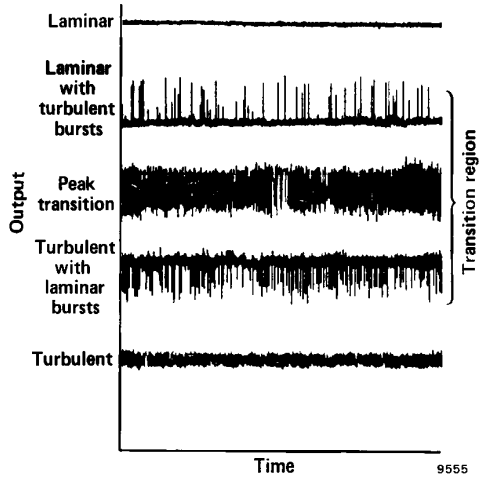

(a) Typical hot-film signals.

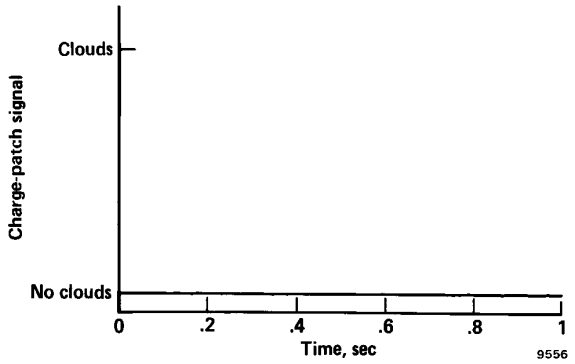

(b) Charge-patch signal.

Figure 26. Hot-film and charge-patch signals without cloud encounters.

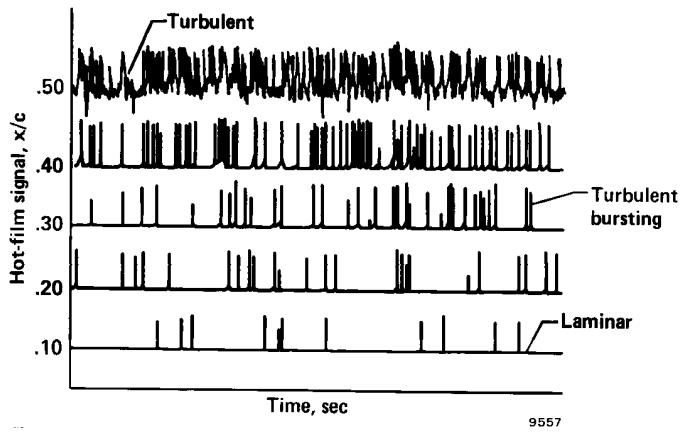

(a) Hot-film signals.

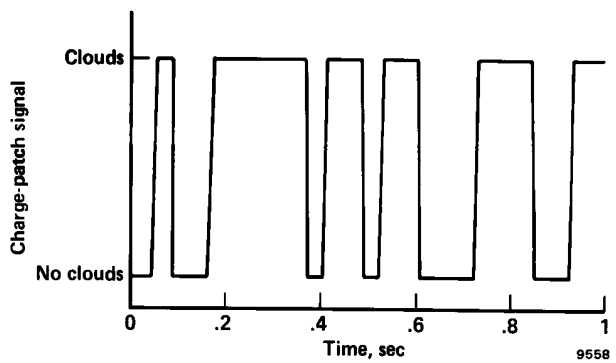

(b) Charge-patch signal.

Figure 27. Hot-film and charge-patch signals with cloud encounters.

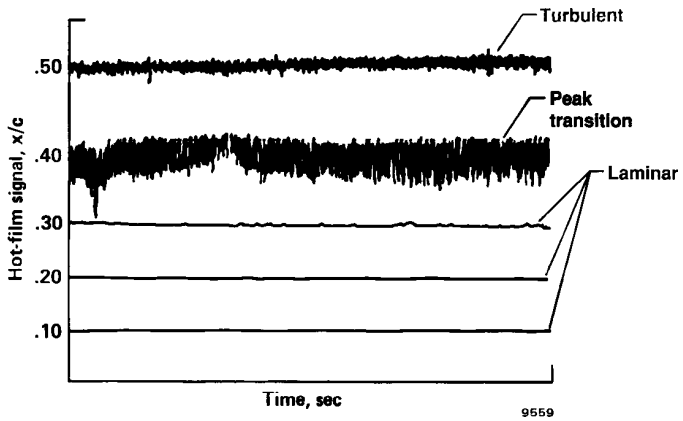

(a) Hot-film signals.

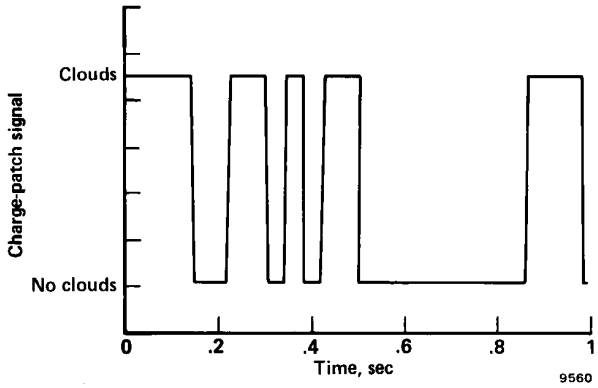

(b) Charge-patch signal.

Figure 28. Hot-film and charge-patch signals with cloud encounters.

NASA
National Aeronautics and Space Administration

Report Documentation Page

1. Report No. NASA TM-101712	2. Government Accession No.	3. Recipient's Catalog No.
4. Title and Subtitle: Effects of Wing Sweep on Boundary-Layer Transition for a Smooth F-14A Wing at Mach Numbers From 0.700 To 0.825		5. Report Date: May 1990
		6. Performing Organization Code
7. Author(s): Bianca Trujillo Anderson and Robert R. Meyer, Jr.		8. Performing Organization Report No. H-1531
		10. Work Unit No. RTOP 505-60-21
9. Performing Organization Name and Address: NASA Ames Research Center, Dryden Flight Research Facility, P.O. Box 273, Edwards, California 93523-0273		11. Contract or Grant No.
12. Sponsoring Agency Name and Address: National Aeronautics and Space Administration, Washington, DC 20546		13. Type of Report and Period Covered: Technical Memorandum
		14. Sponsoring Agency Code

15. Supplementary Notes

This report includes a microfiche supplement attached inside the back cover.

16. Abstract

This report discusses the results of the variable-sweep transition flight experiment (VSTFE). The VSTFE was a natural laminar flow experiment flown on the swing-wing F-14A aircraft. The main objective of the VSTFE was to determine the effects of wing sweep on boundary-layer transition at conditions representative of transport aircraft. The experiment included the flight-testing of two laminar-flow wing gloves. Glove 1 was a cleanup of the existing F-14A wing. Glove 2, not discussed in this report, was designed to provide favorable pressure distributions for natural laminar flow at Mach number (M) 0.700.

The transition locations presented for glove 1 were determined primarily by using hot-film sensors. Boundary-layer rake data was provided as a supplement. Transition data were obtained for leading-edge wing sweeps of 15°, 20°, 25°, 30°, and 35°, with Mach numbers ranging from 0.700 to 0.825, and altitudes ranging from 10,000 to 35,000 ft. Results show that a substantial amount of laminar flow was maintained at all the wing sweeps evaluated. The maximum transition Reynolds number of 13.7×10^6 was obtained for the condition of 15° of sweep, $M = 0.800$, and an altitude of 20,000 ft.

17. Key Words (Suggested by Author(s)): Boundary-layer transition, Laminar flow, Natural laminar flow		18. Distribution Statement: FEDD Subject category 34	
19. Security Classif. (of this report): Unclassified	20. Security Classif. (of this page): Unclassified	21. No. of Pages: 48	22. Price: A03

NASA FORM 1626 OCT 86

Available through NASA's Industrial Applications Centers.